Mechanical Engineering

Proceedings of the 5th Baltic Mechatronics Symposium

Espoo April 17, 2020

Kiviluoma Panu
Kuosmanen Petri
Otto Tauno

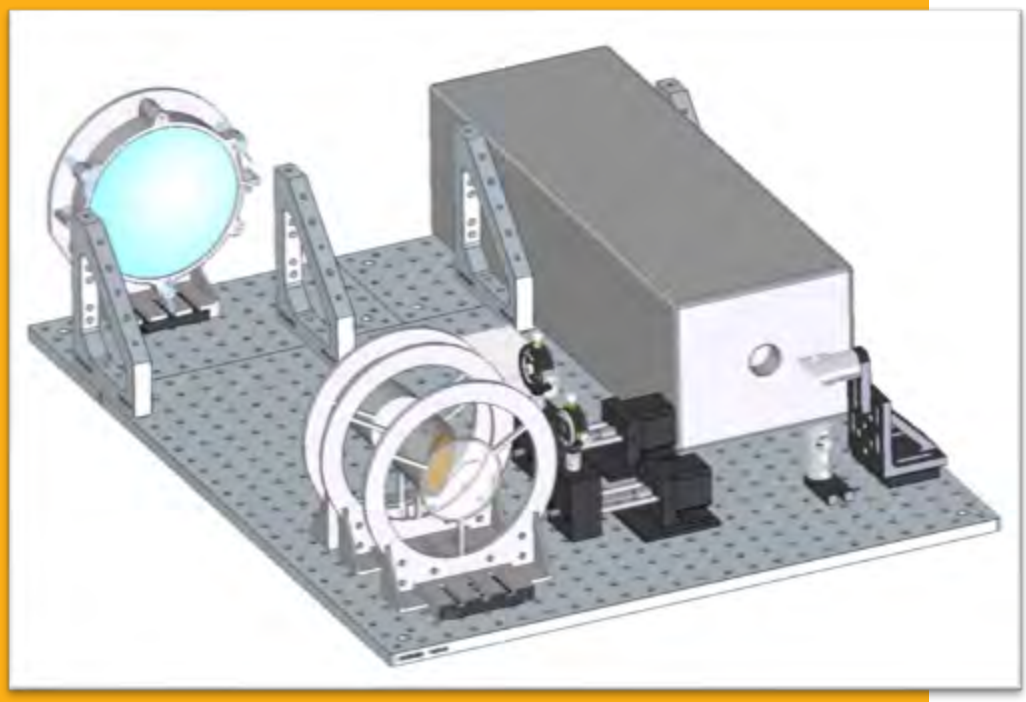

Aalto University
School of Engineering

TAL TECH

Proceedings of the 5th Baltic Mechatronics Symposium

Espoo April 17, 2020

Kiviluoma Panu
Kuosmanen Petri
Otto Tauno

Aalto University
School of Engineering
Mechanical Engineering

Tallinn University of Technology
School of Engineering
Department of Mechanical and Industrial Engineering

Cover image by Jonas Mård, Jonas Rintanen and Verneri Vilmi (Project LIBS)
ISBN 978-952-64-9603-0 (pdf)

Abstract

Aalto University, P.O. Box 11000, FI-00076 Aalto www.aalto.fi
TALTECH, Ehitajate tee 5, 19086 Tallinn, Estonia www.ttu.ee

Author
Kiviluoma Panu, Kuosmanen Petri, Otto Tauno

Name of the publication
Proceedings of the 5th Baltic Mechatronics Symposium
Publisher Aalto University School of Engineering
Unit Mechanical Engineering
Field of research Mechanical Engineering
Language English

Abstract

The Baltic Mechatronics Symposium is annual symposium with the objective to provide a forum for young scientists from Baltic countries to exchange knowledge, experience, results and information in large variety of fields in mechatronics. The symposium was organized in co-operation with Taltech and Aalto University. Due to Coronavirus COVID-19 the symposium was organized as a virtual conference.

The content of the proceedings

1. Monitoring Cleanliness of Public Transportation with Computer Vision
2. Device for Bending and Cutting Coaxial Wires for Cryostat in Quantum Computing
3. Inertial Measurement Method and Application for Bowling Performance Metrics
4. Mechatronics Escape Room
5. Hardware-In-the-Loop Test Setup for Tuning Semi-Active Hydraulic Suspension Systems
6. Newtonian Telescope Design for Stand-off Laser Induced Breakdown Spectroscopy
7. Simulation and Testing of Temperature Behavior in Flat Type Linear Motor Carrier
8. Powder Removal Device for Metal Additive Manufacturing
9. Self-Leveling Spreader Beam for Adjusting the Orientation of an Overhead Crane Load

Keywords Mechatronics, Industrial Internet, Sensors, Actuators, Control
ISBN (pdf) 978-952-64-9603-0
Location of publisher Helsinki
Pages 56

Monitoring Cleanliness of Public Transportation with Computer Vision

Risto Ojala[1,a] Tuomas Kinnunen[,2,b], Joel Mattila[1,c], Mikael Aakko[1,d], Panu Kiviluoma[1,e], and Petri Kuosmanen[1,f]

[1]Department of Mechanical Engineering, Aalto University, Finland

[2]Department of Computer Science, Aalto University, Finland

[a]risto.j.ojala@aalto.fi, [b]tuomas.kinnunen@aalto.fi, [c]joel.mattila@aalto.fi, [c]mikael.aakko@aalto.fi, [c]panu.kiviluoma@aalto.fi, [c]petri.kuosmanen@aalto.fi

Keywords: Computer vision, public transportation, intelligent transportation systems.

Abstract. Due to the ongoing global trend of urbanization, the demand for public transportation is ever-increasing. In order to answer to the growing demand, public transportation vehicles will likely be autonomously operated in the near future, creating a need for advanced surveillance systems. In this study, a computer vision system capable of evaluating the cleanliness of a public transportation vehicle interior is presented. In a laboratory setting mimicking a real vehicle interior, the presented system was studied with a traditional ceiling-mounted wide-angle camera, as well as a linearly actuated camera providing wider visual coverage of the environment. Image data was gathered of the setting in a clean condition as well as containing common trash objects. With this data, the evaluation accuracy of the system was measured with background subtraction, edge detection with random forest, SURF with k-means clustering and XGBoost, and Single-Shot multibox Detector. Single-Shot multibox Detector was found to be the most accurate approach, reaching 95-100% accuracy reliably. The linearly actuated camera was not found to provide notable difference in accuracy compared to the wide-angle camera. Overall, the results indicate that the presented system could be applied in cleanliness monitoring.

Introduction

Autonomous transportation is getting closer to reality each year, especially public transportation vehicles, that are moving on the tracks. As a result of having no staff in the trams, not knowing how dirty it is inside becomes a problem. This is where the need for automatic supervision takes place. Cleaning could be done in certain time intervals, but on-demand cleaning provides higher efficiency, as the vehicle can operate without any unnecessary breaks and less cleaning staff time is used by checking or cleaning already quite clean vehicles. On the other hand, it is best to intervene early to the littering as people are more likely to leave litter in the vehicles that are already dirty.

There are multiple challenges in the automatic cleanliness monitoring system. The main challenge is separating trash from people during vehicle use with sufficient accuracy. In order to be profitable, the systems also need to survive for a long time in vehicle use and not attract vandalism, which implies reliability and robustness constraints.

Cleanliness monitoring with computer vision has been previously studied in different application environments. Rad *et al.* [1] has applied Convolutional Neural Networks (CNNs) to detect individual trash objects on the streets. They experimentally validated the concept by equipping a street sweeper machine with a camera and using the gathered data to train their algorithm, as well as evaluate the accuracy of their approach. In a similar manner, Jayasinghe *et al.* [2] has shown that CNNs can be utilized for evaluating the cleanliness of a public restroom. However, contrary to Rad et al. who performed object detection to locate individual trash, their approach was based on classifying the scenery into different categories.

A camera-based system seems to be the most promising for our system to fulfil accuracy, reliability and robustness requirements. Current methods for the detection of objects include both computer vision techniques and machine learning methods.

The simplest method in terms of implementation is background removal, such as the Gaussian mixture model-based approach of Zivkovic *et al.* [3]. The technique requires sample pictures of the normal state of the scene and later uses them to detect changes compared to the samples. It has been used by Pandit *et al.* [4] to detect unknown objects from surveillance camera feed, by using thresholding in combination with morphological filters of erosion and dilation to reduce noise and improve the boundaries of objects.

A more robust method is to extract edges from images using the methodology presented in the work of Canny [5]. These extracted edge features can be used for classifying the images to required categories. Common approaches for performing this classification include random forest classifiers developed by Breiman [6] and boosting algorithms such as XGBoost by Chen and Guestrin [7].

Speeded Up Robust Features (SURF) by Bay *et al.* [8] is another feature description algorithm partly inspired by the scale-invariant feature transform (SIFT) descriptor made by Lowe [9]. It finds keypoints instead of describing the whole image, which allows the features to be invariant to scaling, translation, and rotation. In addition, they are partially invariant to illumination changes, as well as affine and 3D projection. Classification can be done by using gradient boosting and least-squares methods. Keypoints could also be combined to machine learning methods by using the bag-of-words model, as combined with the k-means clustering method in the study of Sivic and Zisserman [10] for visual search in videos.

Currently popular method, Single Shot MultiBox Detector (SSD) by Liu *et al.* [11], detects objects using a single deep neural network. It outputs object confidence score and bounding box in the image by using classification networks as a base and adding layers for discretizing the box output space to set of default boxes of different sizes and aspect ratios.

This study evaluates the feasibility of applying computer vision units to monitor the interior cleanliness of public transportation vehicles. Two different types of hardware solutions and four different computer vision solutions are implemented and compared based on the accuracy of detecting whether trash is visible in the images.

Methods

Test setup. A test setup was constructed in a laboratory environment by the dimensions of a real public transportation vehicle in Hamburg. The setup has two four-person booths and one double-seat sideways. The dimensions are presented in Figure 1.

There are four separate two-meter long led strips installed in the roof to provide differing cold (6000 K) and warm (3000 K) lighting. The brightness control of each strip is done remotely via WIFI with ESP32 microcontroller. Different light colours and brightness simulate different possible natural light conditions through windows and also changes some shadows and reflections due to different light positions.

Camera Setups. In the test setup, two camera systems were constructed. A wide-angle camera that was similar to commonly applied surveillance cameras and a linearly actuated camera setup with an operational length of 1.2 m. These camera setups were installed above the corridor in the centre of the ceiling and were using different cameras with specifications shown in Table 1. These cameras were connected to small Raspberry Zero W computers.

Data Gathering. Data gathering was done by placing different kinds of trash on the test scene and running a script that automates picture collection from all positions possible with our camera setup. At each camera position, cameras were kept still and the lighting was changed to different scenarios consisting of warm and cold led brightness. The six different cold and warm power percentages used were: $(24, 0), (0, 24), (20, 20), (0, 100), (100, 0), (100, 100)$. The linear rail camera was moved into three or five evenly spaced positions for each trash scenario.

After discussing with officials in the public transportation industry, we found that the most usual trash was food and beverage packaging, like fast food trash, bottles and cans. We gathered approx-

imately 40 different trash objects mainly from this category. After collecting all pictures, they were tagged manually to contain information about whether trash was present and the bounding boxes around the objects. The number of collected images are listed in Table 1.

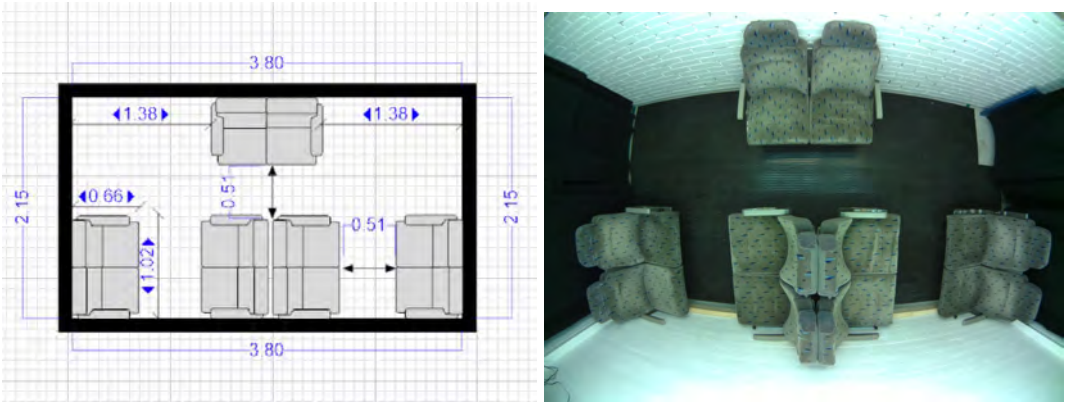

Fig. 1: Constructed laboratory setup.

Fig. 2: Examples of images containing trash. Cropped images were used with certain computer vision methods to eliminate visible changes in the curtains.

Fig. 3: Image of camera setups.

Table 1: Camera and image specifications.

Type	Linear	Wide-angle
Resolution	8 MP	5 MP
FoV vertical	48.8 °	119 °
FoV horizontal	62.2 °	132 °
Collected clean images	176	52
Collected dirty images	756	258
Collected images total	932	310
Average trash per image	3.5	6

Algorithm Specifications and Testing Procedure. Several well-established computer vision techniques were trained and tested with the gathered data to perform an exhaustive comparison. The whole testing process is summarised in Figure 5. The models were trained separately on the images captured from the different cameras.Three train and test splits were acquired randomly from both datasets. Train and test splits contained roughly 80% and 20% of the dataset they were drawn from, respectively. All models were evaluated by training them on a train split and acquiring an accuracy for the respective test split. Accuracy is defined as the number of correct evaluations over the total number of test im-

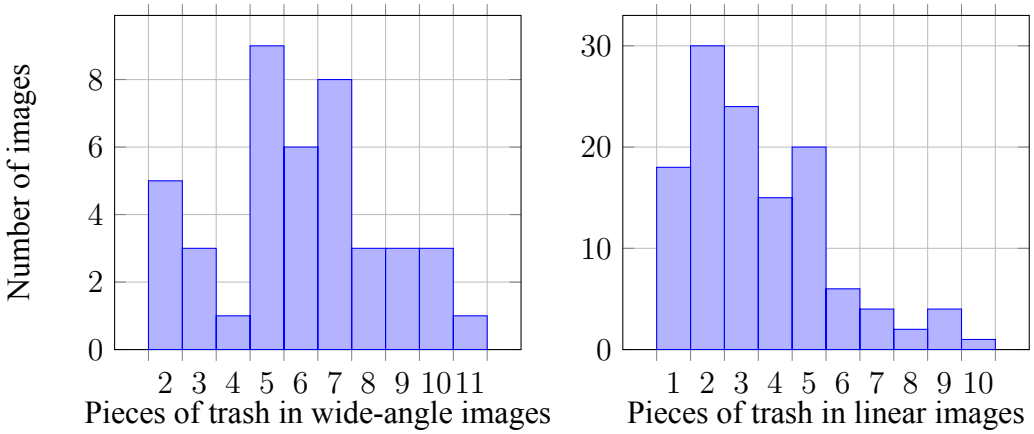

Fig. 4: Histograms of the number of trash objects visible in the images. The linear-rail camera has less trash per image on average. More trash is generally easier to detect.

ages. Each test split was unique, not containing any images in the other test splits. Furthermore, the test splits did not contain differently lit images of the same trash arrangement in the train set.

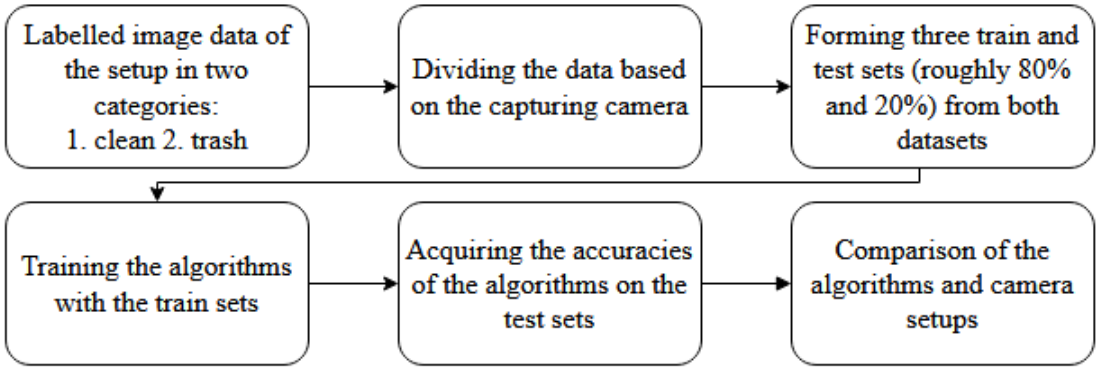

Fig. 5: Flowchart of the testing procedure.

The first applied classification method was background subtraction based on a Gaussian mixture model. A background ratio of 0.99 and 15 mixtures was used in the model. Acquired foregrounds were eroded by a single pixel to remove noise. In order to classify an image to contain trash, a threshold was placed for the foreground over the full image to be larger than 10^{-5}.

A more complex classification method was designed by acquiring visible edges with Canny edge detector, and feeding them to a random forest classifier which outputs the final evaluation. The random forest classifier consisted of 50 decision tree classifiers. For the wide-angle camera, confidence of 60% was required from the random forest to classify an image to contain trash. For the linearly actuated camera, confidence of 50% was sufficient.

SURF was one of the classification methods that was tested, where SURF features were clustered with the K-means algorithm with number of clusters being 100. With the K-means model found, feature vectors could be found by building a histogram of classified keypoints, which then was fed to XGBoost classifier to make predictions for the pictures.

Object detection SSD was used with VGG-16 base network as in the original SSD article [11]. Image input size used was 512x512. Other settings were: cosine scheduler with $T_{max} = 120$, learning rate of 0.001 except for base net 0.0001 and batch size of 5. The training was done five times, and after 200 epochs, the best result was selected across checkpoints from all five runs. Visualisations of applied computer vision methods are presented in Figure 6.

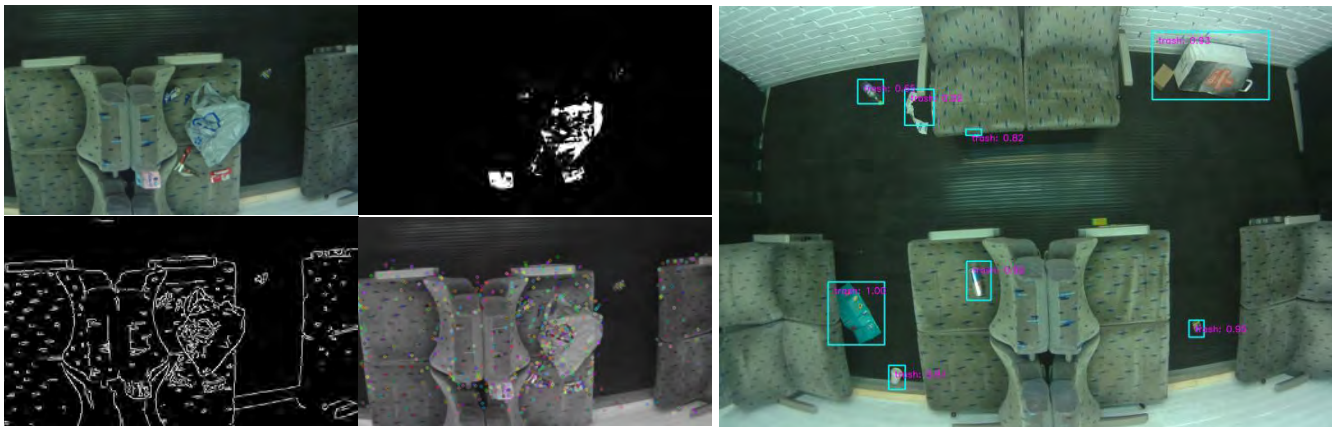

Fig. 6: On the left, from top left to bottom right: original image, background subtraction, canny edge detection and SURF keypoints. On the right: Output of the SSD network.

Results

The accuracies achieved with algorithms on the train-test splits are presented in Figure 7. The presented results showcase that the SSD was superior compared to the other methods, consistently achieving results over 95%. Although all compared algorithms performed well, SURF with k-means clustering and XGBoost did not reach as high accuracies as the others and had the highest variance. Edge detection with random forest had the single worst result with a train-test split, only scoring accuracy of 75%. Overall, the results indicate that the linearly actuated camera does not provide a notable difference in the performance compared to the wide-angle camera.

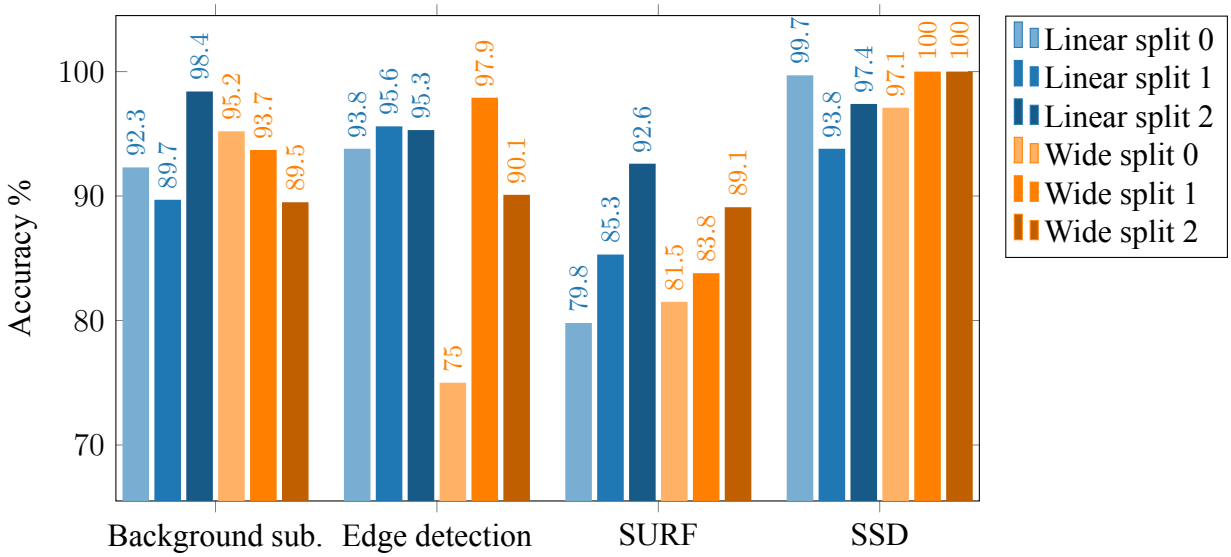

Fig. 7: Accuracies of algorithms categorising images as clean or dirty with different train-test splits of the data.

Conclusion

In this study, a computer vision system for monitoring public transportation cleanliness was developed. The feasibility of the approach was evaluated in a laboratory setup, using a stationary wide-angle camera and a linearly actuated camera with multiple different computer vision algorithms. Acquired results indicate that litter can be accurately detected with computer vision in a public transportation

environment. The linearly actuated camera system was found inconvenient for the application since it did not provide notable improvements in accuracy.

A more reliable comparison of the applied computer vision algorithms could have been made had the gathered dataset contained more images. Especially a higher number of clean images could have influenced the results, as some algorithms found high variance in the clean images. However, the acquired results still indicate that the approach is plausible, and highlight the properties of the compared methods. SSD fared well in our comparison, partly because many images had more than one trash giving it multiple changes to learn or detect a trash object.

The presented application could be extended to distinguish valuable items from litter, and notify the transportation authorities accordingly. Another addition could be to detect people and also monitor their behaviour to prevent violence or other unwanted behaviour.

In the future, such computer vision system could be utilised to improve the customer satisfaction of public transportation, as well as reduce the cleaning costs. Further research of the system will be carried out in real public transportation vehicles. A U-Bahn in Hamburg will be equipped with similar systems, that will be utilised for developing further improvements.

References

[1] M. S. Rad, A. von Kaenel, A. Droux, F. Tieche, N. Ouerhani, H. K. Ekenel, and J.-P. Thiran, "A computer vision system to localize and classify wastes on the streets," in *International Conference on Computer Vision Systems*. Springer, 2017, pp. 195–204.

[2] L. Jayasinghe, N. Wijerathne, C. Yuen, and M. Zhang, "Feature learning and analysis for cleanliness classification in restrooms," *IEEE Access*, vol. 7, pp. 14 871–14 882, 2019.

[3] Z. Zivkovic and F. Van Der Heijden, "Efficient adaptive density estimation per image pixel for the task of background subtraction," *Pattern recognition letters*, vol. 27, no. 7, pp. 773–780, 2006.

[4] T. M. Pandit, P. M. Jadhav, and A. C. Phadke, "Suspicious object detection in surveillance videos for security applications," in *2016 International Conference on Inventive Computation Technologies (ICICT)*, vol. 1, Aug 2016, pp. 1–5.

[5] J. Canny, "A computational approach to edge detection," *IEEE Transactions on pattern analysis and machine intelligence*, no. 6, pp. 679–698, 1986.

[6] L. Breiman, "Random forests," *Machine learning*, vol. 45, no. 1, pp. 5–32, 2001.

[7] T. Chen and C. Guestrin, "Xgboost," *Proceedings of the 22nd ACM SIGKDD International Conference on Knowledge Discovery and Data Mining - KDD '16*, 2016.

[8] H. Bay, T. Tuytelaars, and L. Van Gool, "Surf: Speeded up robust features," in *Computer Vision – ECCV 2006*. Berlin, Heidelberg: Springer Berlin Heidelberg, 2006, pp. 404–417.

[9] D. G. Lowe, "Object recognition from local scale-invariant features," in *Proceedings of the Seventh IEEE International Conference on Computer Vision*, vol. 2, Sep. 1999, pp. 1150–1157 vol.2.

[10] J. Sivic and A. Zisserman, "Video google: Efficient visual search of videos," in *Toward category-level object recognition*. Springer, 2006, pp. 127–144.

[11] W. Liu, D. Anguelov, D. Erhan, C. Szegedy, S. Reed, C.-Y. Fu, and A. C. Berg, "Ssd: Single shot multibox detector," *Lecture Notes in Computer Science*, p. 21–37, 2016.

Device for Bending and Cutting Coaxial Wires for Cryostat in Quantum Computing

Fernando Marquina Magaña[1,a], Antti Honkanen[1,b], Diwakar Gupta[2,c], Ville Nuutinen[3,d], Panu Kiviluoma[1,e] and Petri Kuosmanen[1,f]

[1]Department of Mechanical Engineering, Aalto University, Finland
[2]Department of Electrical and Automation Engineering, Aalto University, Finland
[3]Bluefors Oy, Arinatie 10, 00370 Helsinki, Finland

[a]fernando.marquinamagana@aalto.fi, [b]antti.l.honkanen@aalto.fi, [c]diwakar.gupta@aalto.fi, [d]ville.nuutinen@bluefors.com, [e]panu.kiviluoma@aalto.fi, [f]petri.kuosmanen@aalto.fi

Keywords: bender, Arduino, zigzag, superconductive

Abstract

Quantum computers use quantum mechanical phenomena known as superposition to manipulate and store information. To do this, they rely on quantum bits, or qubits. To maintain the qubits in a stable state the quantum computer must be kept as cold as possible. A cryostat is used to keep the quantum chip in temperatures near absolute zero. Coaxial lines are used to communicate with the quantum chip inside of the cryostat. The coaxials are currently cut and bent manually, which create a bottleneck in production.

In this study a fully automated device was designed for bending and cutting the coaxial wires used in quantum computing cryostats. It is based on Arduino MEGA microcontroller and NEMA 23 size stepper motors. The device is capable of feeding, bending and cutting the coaxial wire automatically according to desired geometry. It is being assumed that the device can meet the demands of cryostat industry that the quantum future needs.

Introduction

Quantum particles can move forward or backward in time, exist in two places at once and even "teleport" [1]. This property of quantum particles is used in quantum computing. Quantum computers can solve problems that are impossible or would take a traditional computer an impractical amount of time to solve [2]. Quantum computers use quantum mechanical phenomena known as superposition to manipulate and store information. To do this, they rely on quantum bits, or qubits. Where a traditional bit is binary and can either hold a value of 0 or 1, qubit can be in a superposition of both. Qubits store information in percentages of probabilities. To maintain the qubits in a stable state and for the quantum computer to work reliably it must be kept as cold as possible. A cryostat is used to keep the quantum chip in temperatures near absolute zero.

This study will deal with the research, design, experimentation and correct tuning of a machine to bend and cut 0.86 mm superconductive CuNi-SCuNi coaxial lines to be used in quantum computer cryostats. These coaxial lines are used to communicate with the quantum chip inside of the cryostat because of their fast data transfer ability and low thermal conductivity [3]. The coaxial lines installed to cryostats have to be bent to withstand the thermal expansion caused by the temperature dropping below 10 mK.

Fig. 1 depicts an open cryostat and the coaxial lines with bent loops can be seen between the level plates. These lines have to be fabricated by hand, but the exponential increase in demand requires automation to take over in the manufacturing of the lines. The main goal of this project is to solve the automation of the bending process. The bending process is currently done by creating a loop and tying it with a cotton thread to eliminate vibration, since the line touching itself would generate an

unacceptable amount of heat (Fig. 2). This phase of manufacturing is extremely time consuming and also the loops require so much space that they do not allow any more lines to be assembled in the same space.

The proposed solution is to bend the wires as shown in Fig. 3. This doesn't only eliminate the vibration and tying but allows for automation and expandability of production. With this shape it is possible to fit multiple lines very close to each other without them touching and generating heat. The device created for this project is the desired solution for the problem. One of the main issues this device faces is the fact that the coaxial lines comes from the manufacturer only in a maximum length of 2 meters, so there will always be an extra piece of wire which has to be discarded.

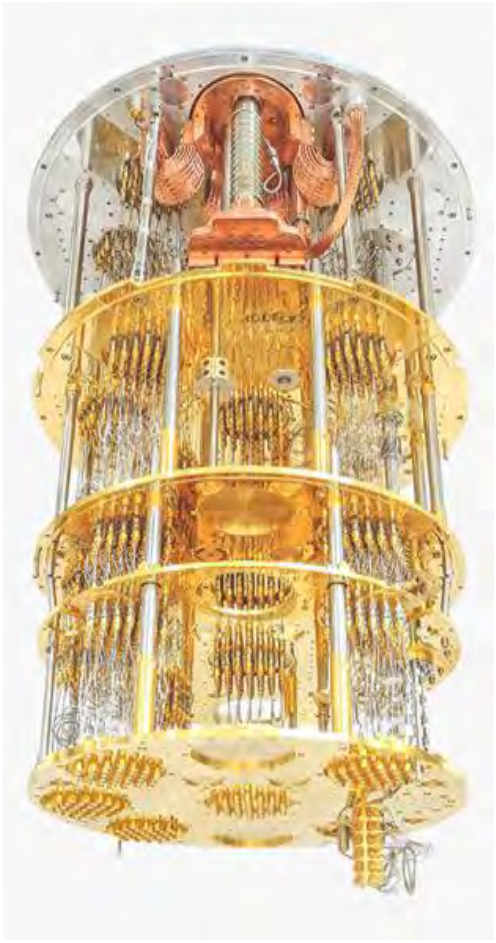

Figure 1. Open cryostat

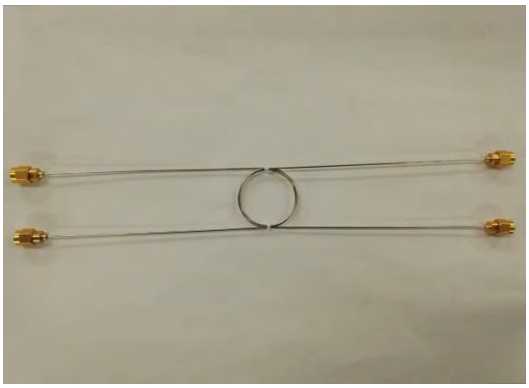

Figure 2. Looped coaxial tied with cotton thread

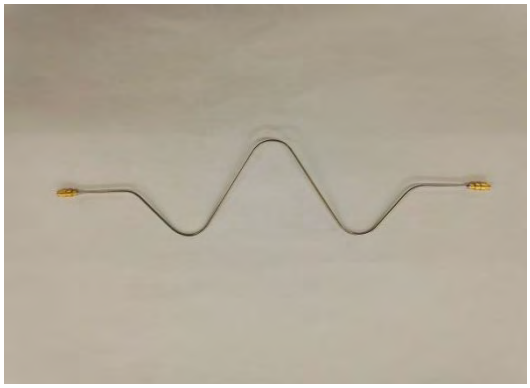

Figure 3. Zigzag bent coaxial

Development of the Device

The device's functions are feeding, bending and cutting. It feeds the coaxial line from the container to itself with the feeder rollers. The coaxial is fed to the bender, which bends the coaxial using a moving pin. The pin pushes the coaxial against the counterpart to bend it. Then the line is fed forward, bent, fed more, bent again and that is repeated until the decided radius for the complete bend is achieved. Then the coaxial is fed until the starting point of the second bend. The pin is moved to the other side of the coaxial, because the next bend will be to the opposite direction than the first was. A bend is created with the same process as the first and this is continued until the coaxial has been bent to the desired geometry.

The first design of the device is presented in Fig. 4. Because of thin coaxial wire and because it was assumed that the feeding wheels should be as close to each other, the device was planned as small as possible, using NEMA 8 stepper motors. As soon as the 3D printed model was ready it became instantly apparent that it was not going to work and that the parts would be too complicated to manufacture because of their small size.

The second step in the design can be seen in Fig. 5. Every part was enlarged and NEMA 14 stepper motors were selected because it was again assumed that the feeding wheels needed to be as close as possible, to consider the remaining piece of the two-meter coaxial line. This design printed fast and it seemed to be a more appropriate size. However, the coaxial lines, even though they are very thin, are extremely stiff, which resulted in the motor torque being too low to achieve the speed and angle desired, unless the motors were pushed to the current limit.

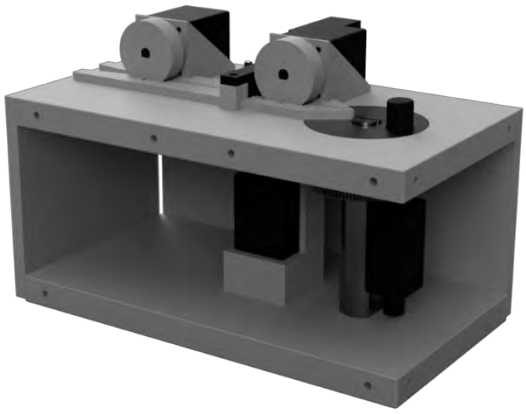

Figure 5. First iteration of the device with NEMA 8 sized stepper motors

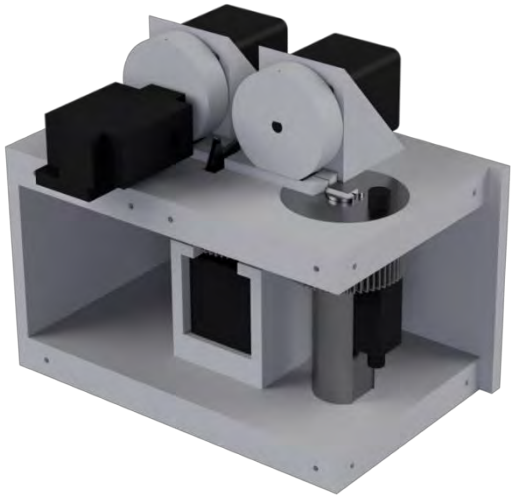

Figure 4. Second iteration of the device with NEMA 14 sized stepper motors

The next iteration of the bender can be seen in Fig. 6 and the final list of selected components is presented in Table 1. One important difference is that the walls of the machine are not part of it anymore, but instead aluminium extrusions are used to hold the machine together and to make it more rigid and easy to access. Bearings were added to the rotating assembly for a smoother operation and reduced friction. An upper support was added to stiffen the rotating assembly and bigger stepper motors were implemented. This last design was more focused in manufacturability with the flat portions being designed to be cut in a water jet out of 6 mm steel plate. The gears and central shaft were made in a way where they can be easily machined, and the stepper motor supports were planned to be 3D printed.

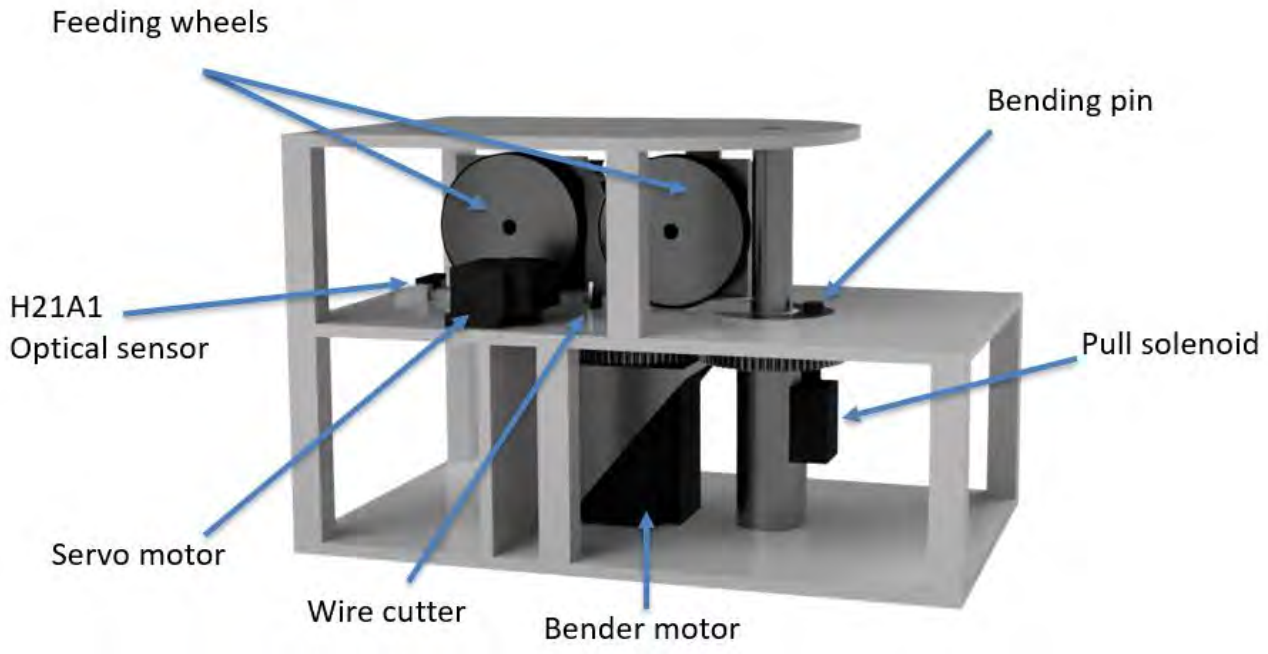

Figure 6. Final design of the device with NEMA 23 sized stepper motors and without walls

Table 1. Components of the final design of the bending device

Component	Specification	Purpose
NEMA 23 Stepper motor x3	3.6 [V], 0.9 [Nm], 1.8[º] step angle (200 steps/revolution)	Move the wire from one position to another and bend the wire.
Arduino microcontroller	MEGA, 54 digital I/O pins	Microcontroller for all electronic components.
Push pull solenoid	12 [V], 5 [N] / 10 [mm]	It pulls the bending pin so it can bend the line from both sides.
H21A1 Optical Sensor	Gap 0.118[’’] (3 [mm]), response time 8 [us]	Computer logic circuitry, detect whenever a new wire enters the machine.
RC Servo motor	Towerpro MG995	Moving the cutter blades.
Power supply	12 [V], 10 [A]	Power source for all electric component.

The device is controlled using an Arduino Mega with RAMPS 1.4 shield attached to it. This allows expandability since it has five stepper motor controllers, four servo motor outputs and a screen to create the UI. In addition, support for configuration is easily accessible.

Stepper motors for bending and feeding are used because of their high torque output at small speeds [4], high precision and compatibility with the controller. A RC servo motor was chosen to power the custom-made blades for the line cutter. A pull solenoid is used to pull the bending pin inside the bender in order to change the direction of the bend.

Since the stepper motors have no feedback and it is not possible to know their absolute position, an optical sensor phototransistor will be used to detect when a new wire enters the machine. The sensor is located before the feeding rollers. This will be complemented with limit switches to be able to calibrate the position of the bender and feeder wheels.

The code for the machine was written in Arduino IDE and it was designed to be easily scalable in case the shape or sizes of the bends would change, the code was separated in smaller functions which can be simply called, for example; bend, feed and cut, this makes it easy to program different lengths of wire and different amount of bends.

The device design is finely tweaked at this point, with no upcoming changes required to increase the functionality, the code is in a rough state and large amounts of testing are required before the expensive coaxial line can be put through. The main point of the project was to increase productivity and quality, which requires time and great attention to the testing phase.

Discussion

This project showed the importance of planning and testing before even starting the design of a machine, not testing the motors and only relying on the spec sheets created a great challenge when the completed machine could not fulfil its purpose. It also demonstrated how important prototyping is compared to only relying on a CAD model in which it is hard to comprehend and visualize the actual size of parts. As next steps the machine will be manufactured to final specs and tested until a fully functioning commercial unit is achieved. This is also only the first phase which the coaxial lines go through in the process to a finished unit, it would be optimal to continue scaling the machine with attachments to strip, solder the connectors and test the signal to ensure quality.

References

[1] Nambu, Y. The Use of the Proper Time in Quantum Electrodynamics I. Progress of Theoretical Physics. 82-94. (1950). doi:10.1143/ptp/5.1.82 [Accessed 22 March 2020]

[2] Arute, F., Arya, K., Babbush, R. et al. Quantum supremacy using a programmable superconducting processor. Nature 574, 505-510 (2019). https://doi.org/10.1038/s41586-019-1666-5

[3] Kushino, A., Kasai, S., Kohjiro, S. et al. Development of Superconducting Coaxial Cables for Cryogenic Detectors. J Low Temp Phys 151, 650–654 (2008) doi:10.1007/s10909-008-9721-x [Accessed 17 January 2020]

[4] Mateusz Kuklaa, Paweł Tarkowskia, Ireneusz Malujdaa, Krzysztof Talaśkaa, Jan Góreckia (2016), 'Determination of the torque characteristics of a stepper motor', Procedia Engineering. [Accessed 22 January 2020]

Inertial Measurement Method and Application for Bowling Performance Metrics

Sampo Laine [a], Topias Turunen [b], Martin Guggemos [c], Kalevi Ekman [d], Panu Kiviluoma [e] and Petri Kuosmanen [f]

[1]Department of Mechanical Engineering, Aalto University, Finland

[a]sampo.laine@aalto.fi, [b]topias.turunen@aalto.fi, [c]martin.guggemos@aalto.fi, [d]kalevi.ekman@aalto.fi, [e]panu.kiviluoma@aalto.fi, [f]petri.kuosmanen@aalto.fi

Keywords: IoT, MEMS, Embedded systems, IMU, Wearable Sensors

Abstract

The current state of bowling performance analysis is focused on the events happening after the ball leaves the hand of the bowler. Typically, the current systems emphasize on the movements of the ball. In this study a different approach was taken, and the measurement system is centered on the movements of the bowler. The feasibility of methods applying inertial measurement systems was evaluated, and the results indicate that adequate performance can be achieved with the low-cost inertial measurement units.

Introduction

Interest in wearable sensors for human activity monitoring is increasing due to recent rapid improvement in microelectromechanical systems (MEMS) technology. The small size and low power consumption of the inertial measurement units (IMU) makes the technology well suited for tracking human movement. The mass production and widespread distribution of MEMS sensors has made a wide variety of low-cost applications feasible [1]. The latest sensor technology has not only improved cost-wise, but also in measurement capabilities. The newest low-cost accelerometers are capable of up to 4 kHz sampling rate in internet of things (IoT) applications, with wireless data transmission [2].

Most of the improvement in the field of MEMS technology is due to their extensive use in mobile devices. Typical smartphone integrated IMU sensors can detect reasonably minute movements, such as handwriting with the edge of a phone [3]. The main difficulties in trajectory tracking with such sensor systems is the inertial measurements tendency to signal drifting, and accumulating error in integration of acceleration data. The magnitude of measurement error varies greatly depending on the quality of the measurement system, though proper signal filtering can be used to diminish the sensor related measurement errors [4].

Multiple approaches for human movement tracking with wearable sensors have been studied in the literature. Biomechanical modelling of the human body can be utilized to greatly decrease the error in trajectory tracking with wearable IMU sensor systems [5]. With multiple sensors, the movement of the entire body can be captured for the analysis of sports performance [6]. Quantification of body pose of an athlete during highly dynamic sports performance is possible with multiple IMU sensors using sensor fusion [7]. For simplistic solutions, just the Kalman filtering based methods for the common three axial accelerometer and gyroscope of an IMU sensor can be used for reasonable results in body orientation tracking [8]. Similar methods have also been considered for bowling performance metrics [9].

The purpose of this study is to further improve the current state of sports performance analytics with wearable inertial sensors. An inertial sensor based low-cost solution for performance analytics in bowling is presented. The measurement system consists of modular wearable IMU sensor-based measurement units. Use of wireless communication methods and microcontrollers are proposed for flexible data transmission and rapid performance feedback for the user during the performance. In addition to trajectory tracking, the system can extract key features of the bowling performance in order to increase the usefulness of the metrics. Validation of the proposed method was conducted with a reference device, and the results were evaluated with experts of the sport.

Methods

In this study, the popular five step method of bowling is considered, which is presented in Figure 1.

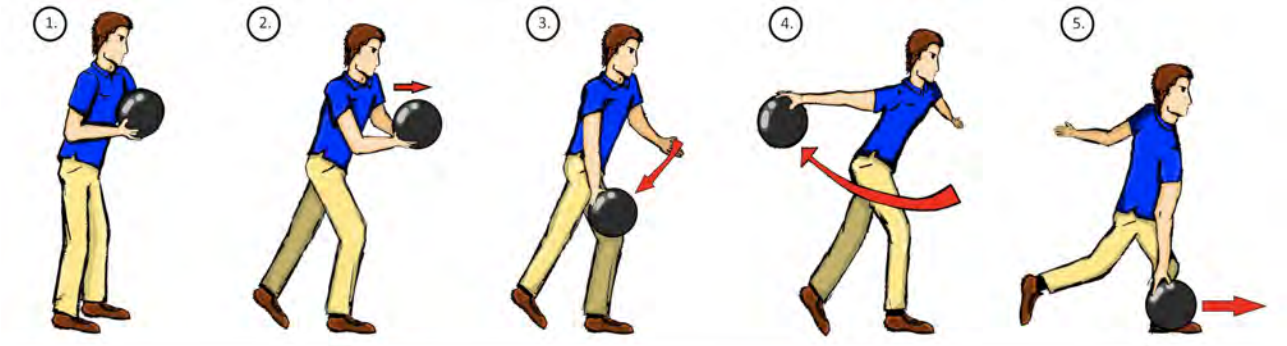

Figure 1. Movement of a bowler using five step method during a shot

The five-step method is broken into five key actions, Figure 1.

1. Starting position: Player holds the ball in his arms, feet close to each other.
2. Push: Player pushes the ball away from his body and takes the first step.
3. Swing: Player swings his arm back, simultaneously stepping forward.
4. Swing peak: Ball reaches the peak position on the swing.
5. Release: Player lets go of the ball.

In order to measure the movement trajectory of the bowler, multiple degrees of freedom of different body parts need to be considered. For this reason, the proposed application concept features a modular sensor unit that can be attached to the body of the bowler. This approach allows multiple configurations for optimization and development of the system in order to yield more useful metrics.

Components of the sensor unit. A wireless modular sensor unit was built for testing the proposed application. The system consists of easily available, low-cost components. Casing for the sensor unit was 3D printed from PLA. Main components of the system are displayed in Table 1.

The ESP32 chip has a dual-core 32-bit microprocessor, built in radio transmitter for WIFI data transmission. The chip has two I2C interfaces, which can be used for communication between the chip and the IMU sensors. One I2C interface can be used to communicate with multiple devices.

Table 1. Components of the sensor unit

Component	Specifications
Adafruit HUZZAH32 ESP32 microcontroller and development board	Processor: 240 MHz Xtensa dual core 32-bit LX6 Wi-Fi: 802.11b/g/n with on board PCB antenna SRAM: 520 KB SPI Flash: 4 MB
MPU6050 IMU sensor	AD-converter: chip built-in 16-bit Gyroscopes range: +/- 250 500 1000 2000 DPS Acceleration range: +/- 2 4 8 16 g
Li-ion battery	Energy capacity: 500 mAh Output voltage: 3.7 V
MicroSD card module and SD card	Memory: 2 GB

An application concept (Figure 2) is presented for the use of the measurement unit which consists of the modular sensor unit and web-based software.

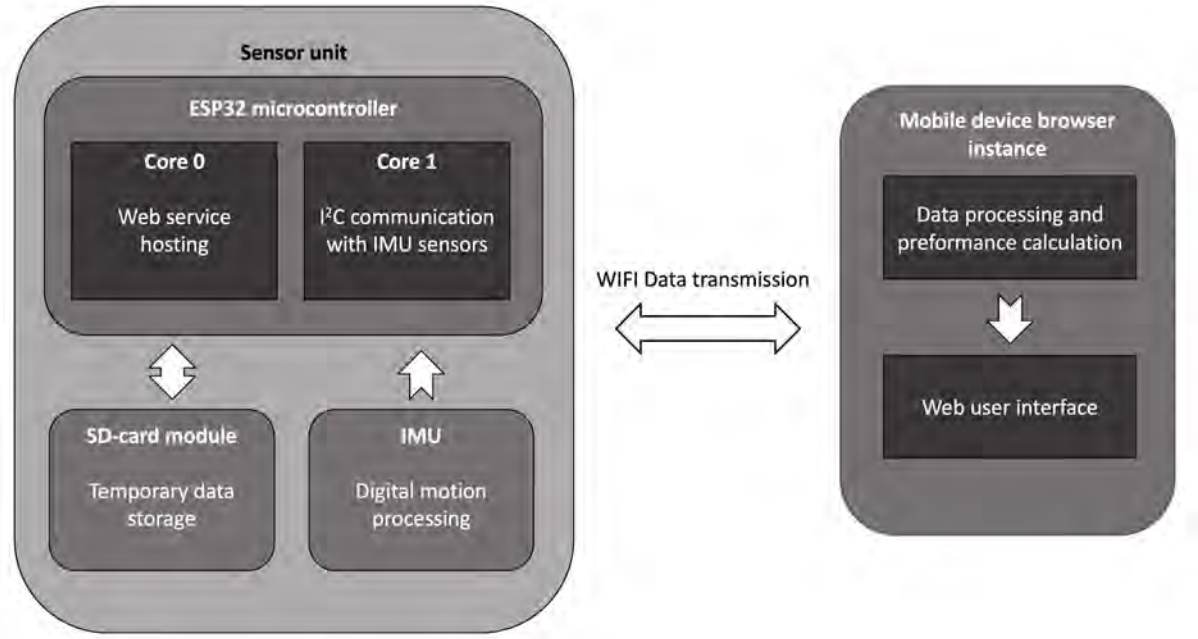

Figure 2. Application concept

The application consists of a wireless modular sensor unit and a web-based user interface, which is designed for mobile devices. The main function of the proposed system is to evaluate the performance of the bowler with numeric metrics, which are derived using the measurement data form the shot. The sensor unit measures movements with an IMU sensor. This design allows for configuration of multiple IMU sensors with I2C communication on the same interface, but the ESP32 chip used has two I2C interfaces, both of which may also be used simultaneously. In this research, only one IMU sensor was used.

Having two processor cores, the ESP32 can run two parallel tasks. The concept leverages the parallelization by serving the web software on one core, and the I2C communication with the IMU sensor on the other core. Transmission control protocol (TCP) WebSockets are used in the data

transmission through Wi-Fi to the mobile device. Due to the memory limitations of the ESP32, an external SD-card module is used for intermittent data storage. For short measurements, the volatile memory of the ESP32 may also be used.

The static website content is stored in the SPIFFS memory of the ESP32 and can be sent to the client when the client connects to the sensor unit. This approach enables effective data processing, since the far more capable CPU of the mobile device can be used for extracting the definitive metrics from the data.

Reference device and test setup was built in order to determine the suitability of the IMU sensor for tracking dynamic movements of the human body. The device is presented in Figure 3. The setup consisted of a pendulum with two degrees of freedom, modelling the elbow joint of a bowling person. With a rotary encoder on the main rotating axis, the pitch of the pendulum was measured with high accuracy.

An IMU sensor was attached to the tip of the pendulum, and an ESP32 microcontroller was used for the data acquisition, similarly to the real use-case with the proposed sensor unit. The device features two rotary encoders, of which only one was used due to limitations of the microcontroller chip.

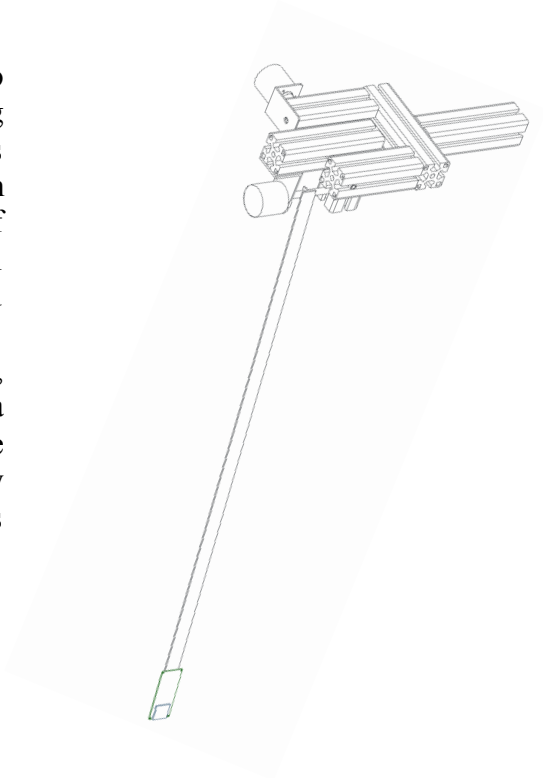

Figure 3. 3D model of the reference device

Measurement procedures. The sensor unit was slightly modified to enable the measurements. Wireless communication was not used in order to simplify the measurement procedure and in addition to the IMU sensor, an incremental rotary encoder with 2000 PPR resolution was parallelly measured on the ESP32 for reference. The results were directly written to a file on a computer using universal asynchronous receiver-transmitter (UART) connection.

Figure 4. Measurement process flow

Multiple measurement cases with varying sideways rotations were created with the reference device. The measurement flow (Figure 4) represents one of the measurements. Same principal steps were reproduced on each repetition. The duration of one measurement was between 5 and 15 s, representing the length of a bowling shot. Varying amount of sideways rotation was applied during the measurements in order to simulate the human body movements.

Signal processing and algorithms. The built-in digital motion processing of the MPU6050 chip was used for the sensor fusion, which is capable of directly outputting Euler angles, and gravity

compensated acceleration data. Simple rotation matrices could be used for transforming the Euler angles to cartesian coordinates. Similarly, basic matrix algebra can be applied in order to determine the reference position of the sensor with the encoder data.

Results

Results of the measurements are displayed in Figures 5 and 6. The pre-processed yaw, pitch and roll data directly from the IMU sensor data is plotted against the reference data from the encoder. During heavy shaking (Figure 5), the largest error in pitch angle was 17 degrees, and 6 degrees during minor shaking (Figure 6). Reference for yaw and roll was not measured.

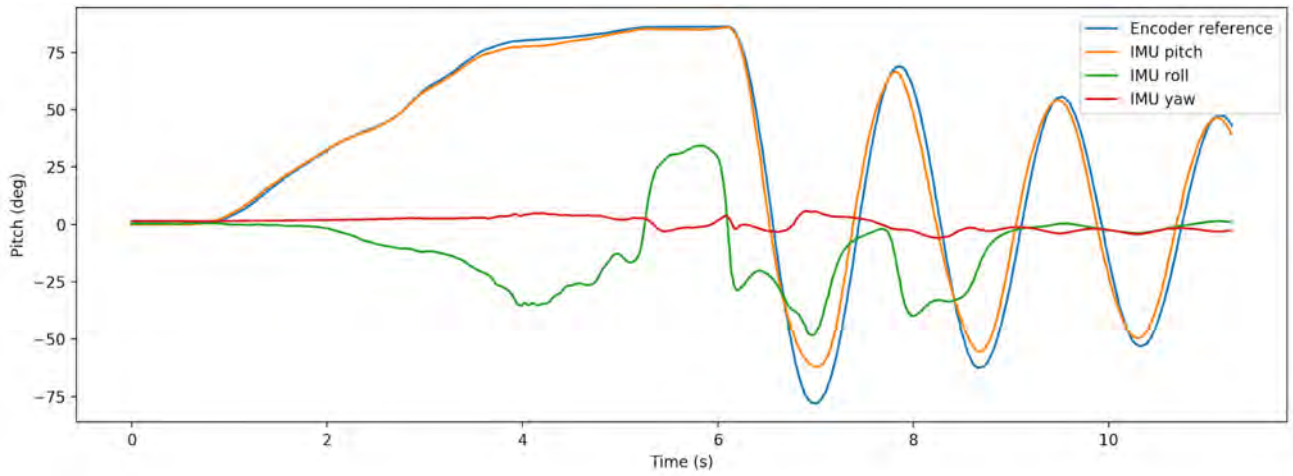

Figure 5. Reference measurement with heavy shaking

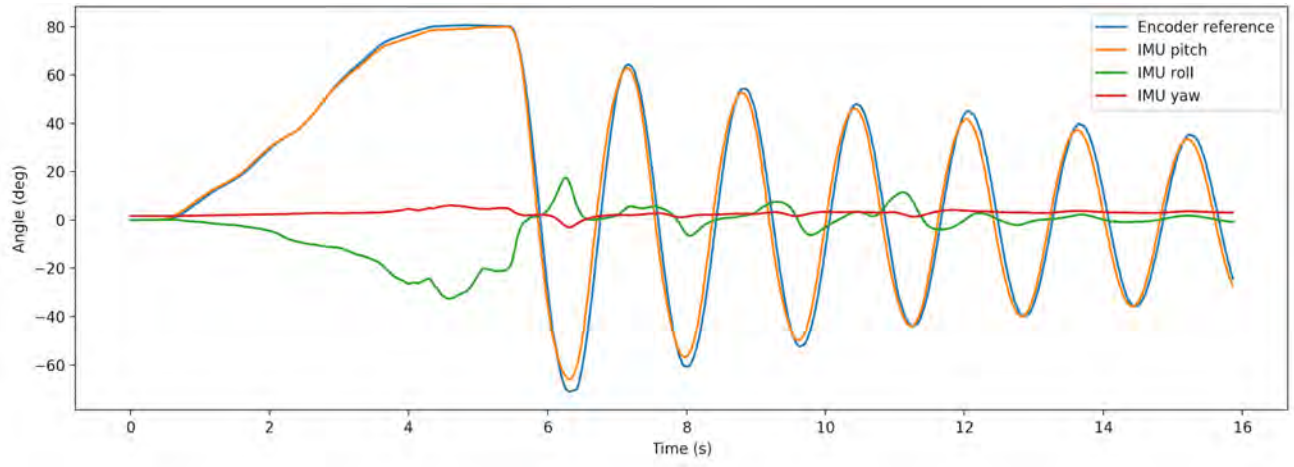

Figure 6. Reference measurement with minor shaking

Discussion

The results imply that the developed sensor system can detect fast dynamic movements. Information of the movement can then be used to extract various performance characteristics from the data, and the described application concept can be used to give accurate feedback to the user. According to a bowling expert, the achieved accuracy of the sensor is enough to give informative feedback about the shot, however more practical testing is needed for confirmation. With the enough sensors attached to

the body, the system could be developed to determine the pose of the bowler, yielding even more informative metrics.

The proposed sensor unit and application concept are not limited for use in bowling, but the system could also be used in different body orientation or movement tracking scenarios. All the components used in the sensor system are cheap and easily available for anyone, making this research a platform for versatile future development.

References

[1] Mukhopadhyay, S. C. (2015) 'Wearable sensors for human activity monitoring: A review', IEEE Sensors Journal, 15(3), pp. 1321–1330. doi: 10.1109/JSEN.2014.2370945.

[2] Koene, I., Viitala, R. and Kuosmanen, P. (2019) 'Internet of Things Based Monitoring of Large Rotor Vibration with a Microelectromechanical Systems Accelerometer', IEEE Access, 7, pp. 92210–92219. doi: 10.1109/ACCESS.2019.2927793.

[3] Pan, T.-Y. et al. (2018) 'Handwriting Trajectory Reconstruction Using Low-Cost IMU', IEEE Transactions on Emerging Topics in Computational Intelligence. IEEE, 3(3), pp. 1–10. doi: 10.1109/tetci.2018.2803777.

[4] Siciliano, Bruno, Khatib and Oussama (2008). 'Springer Handbook of Robotics' Springer Science & Business Media, ISBN 9783540239574

[5] Fasel, B. et al. (2018) 'Joint Inertial Sensor Orientation Drift Reduction for Highly Dynamic Movements', IEEE Journal of Biomedical and Health Informatics. Institute of Electrical and Electronics Engineers Inc., 22(1), pp. 77–86. doi: 10.1109/JBHI.2017.2659758.

[6] Fasel, B. et al. (2017) 'Validation of functional calibration and strap-down joint drift correction for computing 3D joint angles of knee, hip, and trunk in alpine skiing', PLoS ONE. Public Library of Science, 12(7). doi: 10.1371/journal.pone.0181446.

[7] Yoshioka, S. et al. (2018) 'Pose tracking with rate gyroscopes in alpine skiing', Sports Engineering. Springer London, 21(3), pp. 177–188. doi: 10.1007/s12283-017-0261-y.

[8] Ahmed, H. and Tahir, M. (2017) 'Improving the Accuracy of Human Body Orientation Estimation With Wearable IMU Sensors', IEEE Transactions on Instrumentation and Measurement. IEEE, 66(3), pp. 535–542. doi: 10.1109/TIM.2016.2642658.

[9] Tung Mun Hon, Arosha, S. and Nick, F. (2009) Biomechanical Analysis of 10-Pin Bowling Using Wireless Inertial Sensor. IEEE

Mechatronics Escape Room

Vili Juustila[1, a], Jani Vihko [1,b], Tuukka Uimonen[1,c], Panu Kiviluoma[1,d] and Petri Kuosmanen[1,e]

[1]Department of Mechanical Engineering, Aalto University, Finland

[a]vili.juustila@aalto.fi, [b]jani.vihko@aalto.fi, [c]tuukka.uimonen@aalto.fi, [d]panu.kiviluoma@aalto.fi, [e]petri.kuosmanen@aalto.fi

Keywords: puzzles, learning, motivation

Abstract

Due to their engaging nature, escape rooms are an interesting alternative teaching method. Studies in other fields have shown educational escape rooms to improve motivation and learning. As many conventional escape room puzzles are mechatronic, the concept should also work well for educational purposes in engineering. In this study, an escape room with three mechatronic puzzles is created. The puzzles are designed for high-school students with a combined time limit of 10 minutes. The results are presented as 3D models of the puzzles along with extensive descriptions. A participant survey to analyze the results of the room is also described.

Introduction

Escape rooms are games in which participants solve puzzles placed inside a room in order to achieve a goal - usually, getting out of the room. These games have risen in popularity particularly during the 2010s. Simultaneously, demand for engineers in Finland has also increased, and new ways to attract people to take on engineering studies are sought. As escape rooms usually include puzzles that utilize mechatronics themselves, their suitability for teaching the basic principles of mechatronics and motivating potential students poses many possibilities. In other fields, there has also been interest in using escape rooms in teaching due to the co-operative and engaging nature of the game [1].

In the field of mechatronics, similar tools such as remote laboratories [2] and puzzle-like modular components [3] have been studied, but so far, escape rooms have only been utilized in other fields. For example in the nursing field, students that participated in a "Nursing escape room" believed that it helped them learn the subject, as well as motivated them to study. [4] An educational escape room for pharmacy students produced similar results, as students showed statistically significant increases in knowledge after completion of the game. [5]

The aim of this study is to develop an escape room with three puzzles for use in demonstrating common mechatronic principles, such as gear trains, remote control and system identification. With a short completion time limit of 10 minutes, the main goal is to motivate potential students to take on technical university studies rather than teach new concepts. To evaluate the impact of the room, short questionnaires were developed to be filled by the participants before and after the game. Data from the questionnaires can be analyzed to find if the room improved motivation, and if the improvement happened also for people who originally were not very interested in the field. Before entering, the questions focus on success in studies and previous interest in the field, while questions after the game focus on the escape room experience.

Methods

Setting. The mechatronic escape room was constructed inside an office room at the Aalto Industrial Internet Campus in Espoo, Finland. Inside the room, three different mechatronic devices function as puzzles. These puzzles have to be completed in numerical order, starting from puzzle 1. Puzzles 2 and 3 are locked in the beginning of the game and players can unlock them after completing the previous puzzle. After completing puzzle 3, players gain access to a key, which opens the exit door and ends the game. The game can be played in groups of 2-6 persons, with the optimal group size being four. Players are given a time limit of 10 minutes to complete all three puzzles and exit the room.

Design. As opposed to the usual time limit of around one hour, our time limit of 10 minutes requires the puzzles to be relatively straightforward. The room being aimed for high school students and prospective university students, the puzzles should ideally utilize only high school level physics or mathematics but also have some relevance in university studies. In the general design, "a danger in using the trappings of escape games, such as boxes with combination locks, is that designers can focus too heavily on "unlocking boxes" as the primary goal instead of exploring a narrative" [1].

Another consideration is that the puzzles should use the advantage of having a hands-on environment, rather than just revealing a new set of equations to solve after completing previous ones. With our time limit, the puzzles should be easily understandable, as opposed to the usual mystery of finding the puzzle itself. The common escape room experience of mystery can still be maintained using different kinds of cheat sheets [6] that can reveal more information if in doubt. If possible without spoiling aforementioned mystery, plenty of instructions should be given beforehand in order to efficiently use the given time limit.

Puzzle 1. The first puzzle is intended to demonstrate capabilities related to Internet of Things (IoT), digitalization and remote control, as well as motivate participants by involving video streaming as an everyday phenomenon into engineering problems. A smartphone is used for the remote control, which is an important and reliable device for most of the target group. The mechanical components of the puzzle are also left visible to show the mechanical and practical aspects of the puzzle.

Puzzle 2. The second puzzle demonstrates mechanics, in particular gear ratio selection. As such, it shows the participants the importance of simple mechanisms, and rewards them through making the machine operational. The participants gain hands-on experience on building and using a simple mechanism, as well as practical experience on gears and mechanics.

Puzzle 3. The last puzzle shows high school physics in action, making theory into something concrete. It also encourages system identification, as the puzzle is difficult to solve with random attempts. The main motivator is the connection of familiar concepts with real-life phenomena and practical mechatronics.

Participants. The escape room was designed mainly for high school students and other participants with similar knowledge or backgrounds. The puzzles are designed to motivate high school students and utilize concepts that should be understandable with high school level knowledge. Other groups, such as other second degree level, upper comprehensive school and university students, as well as professors etc. can also attend. However, these groups might find the difficulty level to be either too high or too low, as well as have problems with increasing their motivation regarding mechatronics.

Participant survey. In order to evaluate the feasibility of an escape room as a form of mechatronics teaching, participants are asked to complete a short survey before and after the game. The data can be then analyzed demographically. The pre-game survey consists of three claims intending to chart knowledge in the field and future study plans:

1) I've had good academic success in physics and mathematics
2) I have practical experience in mechanics or electronics (e.g. related hobbies)
3) I am considering studying engineering in the future

The post-game survey consists of five claims, which focus on the escape room experience to find out which particular factors would contribute to improving motivation:

1) I enjoy going to escape rooms
2) The escape room puzzles were interesting
3) Knowledge of physics or mathematics helped me in the puzzles
4) I enjoy hands-on working similar to solving puzzles
5) The escape room motivated me to apply for further studies

The responses to the claims are assessed on a 5-point Likert-type scale, with 5 corresponding to totally agree and 1 corresponding to totally disagree.

Results

Final design of the puzzles. The final design of the puzzles was done by using 3D CAD modelling software as well as the design guidelines described in the design chapter. The models are sketches and have deliberate nonspecificity in order to make small design changes possible during building. All of the puzzles utilize microcontrollers and motor drivers, as well as electric motors. Puzzle 1 uses two servo motors and a stepper motor, while puzzles 2 and 3 use DC motors.

Puzzle 1. The puzzle consists of a web camera placed on a tray, which moves on a linear guide rail. The position of the camera tray (movement, rotation & tilting angle) can be adjusted using an IoT platform called Blynk, which is preinstalled in a mobile phone placed inside the room. The assembly is placed inside a sealed box and users have to find clues inside it by changing the angle and placement of the camera using Blynk. In order to see inside the box, live video feed from the web camera is shown on a screen placed next to the box. Participants can see the camera and mechanical components of the assembly through a small window, so that the relationship between camera movement and smartphone controls can be figured out. The clues are located on the inside wall of the box and cannot be seen from the window. After finding all the clues and solving the puzzle, a number lock can be opened. Inside the number lock there is a key, which can be used to access the next puzzle. A CAD model of puzzle 1 can be seen in figure 1.

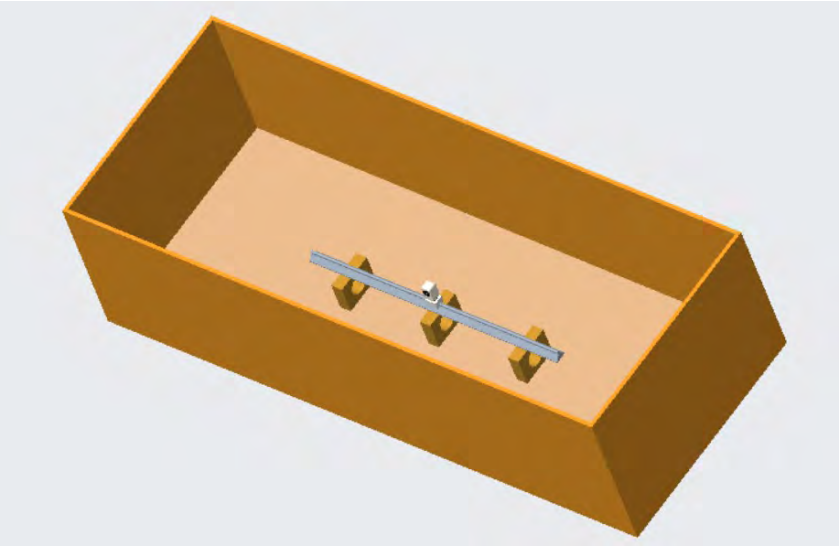

Figure 1. CAD model of puzzle 1. The web camera and linear guide rail are placed inside a sealed box, operated remotely from a smartphone. Clues are placed on the inside walls of the box.

Puzzle 2. The key from the previous puzzle can be used to open a locker, where the user will find a timing belt and six matching pulleys. The puzzle itself has a DC motor and an empty freely rotating shaft. The DC motor runs at a constant speed when a momentary button is pushed. The user must insert the right combination of pulleys into the assembly in order to achieve the requested speed at the freely rotating shaft. This velocity is measured by an encoder and the current rotational velocity is shown on an LCD screen. When the correct combination of pulleys is set, the assembly will move a lever mechanism that releases the key to open the next puzzle. A CAD model of puzzle 2 can be seen in figure 2.

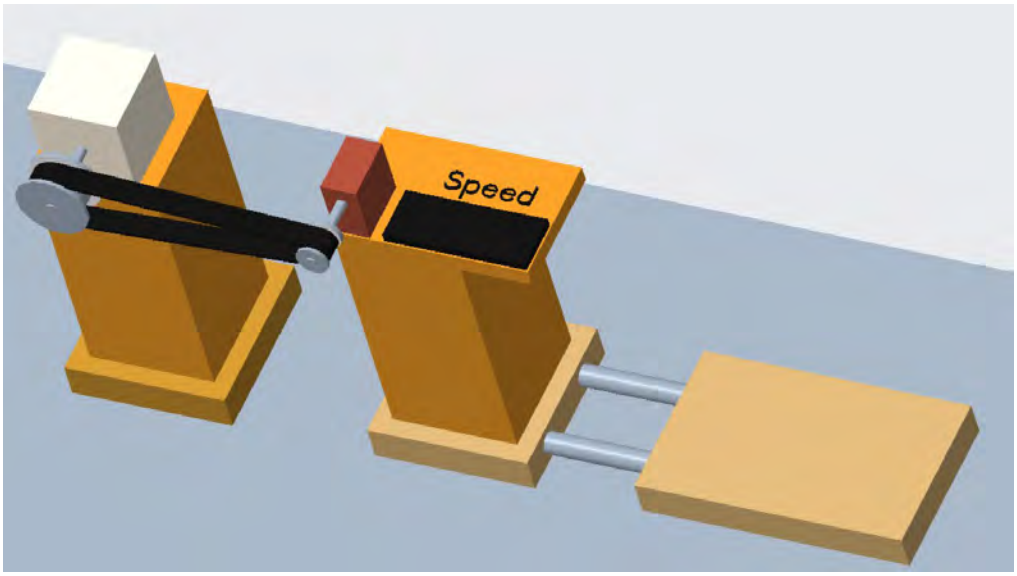

Figure 2. CAD model of puzzle 2. The DC motor is connected to the freely rotating shaft with a timing belt and pulleys. The design allows small horizontal movement of the shaft in order to fit different size pulleys with only one timing belt. The belt is kept tight with a spring system.

Puzzle 3. The key received from puzzle 2 fits to a locked box, which has an adjuster for an encoder and a release button inside. The puzzle itself is similar to a small minigolf track. After opening the box, players are able to set the angle of a pendulum, which acts as a minigolf club. The angle is set using the encoder adjuster. When the angle has been set, the release button releases the club and the club will hit a ball causing an impulse. The task is to adjust the club to the correct angle, which will result in the ball landing inside a hole at the end of the track. The purpose of this puzzle is to help the user understand how the club's potential energy transforms into the ball's kinetic energy and that the release height of the club is the exact same height as the hole minus losses (friction between the ball and the surface). When the ball enters the hole, it will release a key for the last door of the escape room. A CAD model of puzzle 3 can be seen in figure 3.

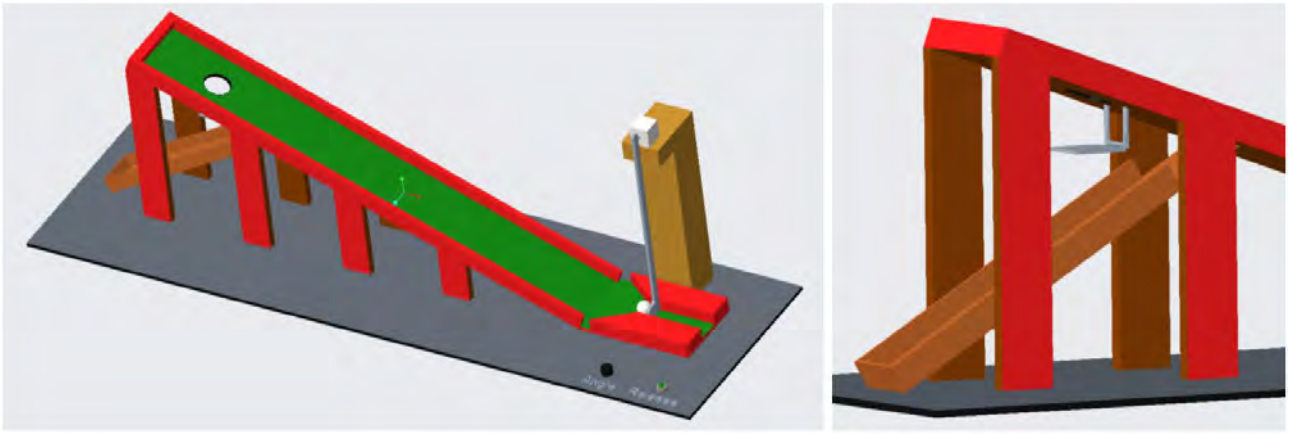

Figure 3. CAD model of puzzle 3, which resembles a small minigolf track. After the angle for the club is set, it will fall freely and strike the ball. If the angle is set correctly, the ball will fall inside the hole and drop the key placed on the mechanism (right) into the trough.

Discussion

Analyzing the puzzles, the time limit of 10 minutes proves to be very restricting in terms of puzzle design. Especially with three puzzles, the problems have to be simple enough to consist mostly of using high-school physics rather than learning new things, which could have a significantly higher impact on motivation. Having only one, more complicated puzzle might achieve this better, but we feel that the escape room format still lends itself better to longer time periods of at least half an hour.

Suitable participants can be invited to the escape room in individual 2-6 person groups or in larger batches of said groups. However, for optimal data gathering and efficiency, the escape room should be organised in a larger public event, for example as part of a student or engineering convention. With the time limit of 10 minutes and an optimal group size of four, an eight hour convention could result in up to 96 participants (this number includes set-up times, breaks etc.).

If the results (from both practical aspects and from the survey) gained from a public event etc. turn out as positive, future uses could include expanding and further developing the escape room. This could include for example developing the existing puzzles according to the data gathered, as well as adding more puzzles to the room. Modern escape rooms typically consist of multiple rooms, which would add to the experience. Expanding the space would be necessary especially if more puzzles were to be added. In any case, expanding or further developing the room would most likely have to include expanding the duration of the game. By extending the duration, the escape room could also be used for teaching purposes, not only for motivation. More time would allow for more complicated puzzles and concepts, which in turn would encourage a deeper thinking process while completing the puzzles.

References

[1] Nicholson, S., 2018. Creating Engaging Escape Rooms for the Classroom. *Childhood Education*, vol. 94, no. 1, pp. 44-49. Available from: https://www.tandfonline.com/doi/full/10.1080/00094056.2018.1420363 ISSN 0009-4056. DOI 10.1080/00094056.2018.1420363.

[2] C. M. Ionescu, E. Fabregas, S. M. Cristescu, S. Dormido and R. De Keyser, 2013. A Remote Laboratory as an Innovative Educational Tool for Practicing Control Engineering Concepts. *IEEE Transactions on Education*, vol. 56, no. 4, pp. 436-442. doi: 10.1109/TE.2013.2249516

[3] K. Asato, K. Asato, T. Nagado and S. Tamaki, 2015. Development of low cost educational material for learning fundamentals of mechatronics. *2015 International Conference on Intelligent Informatics and Biomedical Sciences (ICIIBMS)*, Okinawa, pp. 454-456. doi: 10.1109/ICIIBMS.2015.7439526

[4] Gómez-Urquiza, J.L., Gómez-Salgado, J., Albendín-García, L., Correa-Rodríguez, M., González-Jiménez, E.and Cañadas-De la Fuente, Guillermo A., 2019. The impact on nursing students' opinions and motivation of using a "Nursing Escape Room" as a teaching game: A descriptive study. Available from: http://www.sciencedirect.com/science/article/pii/S0260691718309146 ISBN 0260-6917. DOI 10.1016/j.nedt.2018.10.018.
[5] Eukel, H.N., Frenzel, J.E. and Cernusca, D., 2017. Educational Gaming for Pharmacy Students - Design and Evaluation of a Diabetes-themed Escape Room. *American Journal of Pharmaceutical Education*, Sep, vol. 81, no. 7, pp. 6265-5. Available from: https://www.ncbi.nlm.nih.gov/pubmed/29109566 MEDLINE. ISSN 0002-9459. DOI 10.5688/ajpe8176265.
[6] Nicolas Dietrich, 2018. Escape Classroom: The Leblanc Process-An Educational "Escape Game". *Journal of Chemical Education*, Jun 12, vol. 95, no. 6, pp. 996. Available from: https://pubs.acs.org/doi/abs/10.1021/acs.jchemed.7b00690 ProQuest One Literature. ISSN 0021-9584. DOI 10.1021/acs.jchemed.7b00690

Hardware-In-the-Loop Test Setup for Tuning Semi-Active Hydraulic Suspension Systems

Heikki Lu[1,a], Elisa Alboni[1,b], Ville Björklund[1,c], Matti Lin[1,d], Jyrki Kajaste[1,e], Panu Kiviluoma[1,f] and Petri Kuosmanen[1,g]
[1]Department of Mechanical Engineering, Aalto University, Finland
[a]heikki.lu@aalto.fi, [b]elisa.alboni@aalto.fi, [c]ville.bjorklund@aalto.fi, [d]matti.lin@aalto.fi,
[e]jyrki.kajaste@aalto.fi, [f]panu.kiviluoma@aalto.fi, [g]petri.kuosmanen@aalto.fi,

Keywords: Single board computer, Raspberry Pi, Simulink, Real-time system, Simulation

Abstract

Suspension is an important vehicle system because it provides steering stability with good handling and comfort in different road conditions. Among the various types of suspension system, semi-active hydraulic suspension systems are becoming increasingly popular since they require minimal energy to be driven while offering very good performance compared to other solutions. The damping coefficient of semi-active dampers can be varied by adjusting the spool inside the proportional valve. To obtain the desired performance and damping force, a proper control system should be created and tested. However, currently testing and tuning suspension systems are time consuming and expensive and software-only simulations are not very accurate due to phenomena like fiction and hysteresis. This study proposes a light and cost-effective single board computer (SBC) based hardware-in-the-loop (HIL) simulation test setup for testing and tuning semi-active suspension systems. Another goal for test setup is improving usability of control units of HIL systems. The hydraulic test bench was built and tested by driving it through Raspberry Pi (RPi). The necessary signal processing circuits were developed and tested separately from the system. The IoT capabilities of the RPi were also validated by uploading and running Simulink model on the board and tuning model parameters during control system simulations.

Introduction

Hydraulic dampers are widely employed in the suspension system, especially on heavy vehicles, in order to provide good vibration isolation, high ride comfort level and better handling stability [1]. However, they suffer from a significant disadvantage due to the change in high-frequency characteristics. In order to mitigate the consequent negative effects, semi-active control strategies for hydraulic dampers have been developed to enhance the performance of passive suspensions [2].

Semi-active hydraulic suspension systems are becoming more widely used because they require minimum amount of energy to function and they exhibit good performances [3]. In fact, in semi-active damping systems, the damping coefficient can be varied, and the desired damping force can be obtained by adjusting the spool displacement of an electro-hydraulic proportional valve [4].

In order to obtain the characteristics of a suspension system it is necessary to simulate the suspension system, but there are several challenges associated with the simulation process. Several simulation models have been developed to test hydraulic suspension systems, but the results of the simulations are relatively inaccurate. Phenomena like friction or hysteresis of the damper are very difficult to accurately simulate using software. On the other hand, testing the real process has proved to be difficult, expensive or time consuming. [5]

Hardware-in-the-loop (HIL) simulation is an alternative which offers various benefits. HIL simulation system is a simulation system where some of the control-loop components are replaced by real hardware in order to get more accurate results. The HIL-system requires less time and costs compared to both software-only simulation system and real process simulation [5]. HIL simulations have been widely used in industry to simulate suspension systems of heavy vehicles [6].

HIL simulations are commonly made using high-performance electronic platform Field-programmable gate arrays (FPGA) [7]. However, the FPGAs require PC add-on cards for efficient

communication interfaces for simulation which are significantly more costly than single board computers (SBC) such as Raspberry Pi (RPi) boards. In fact, the same study showed that the cheap and relatively easy-to-use RPi meets the requirements of real-time simulation.

Another benefit of using RPi as main hardware for HIL simulation control is MATLAB support for Simulink block diagram environment for modeling the simulation system. The tool makes the development and tuning of the algorithms for simulations more convenient and efficient. In addition, the support package enables IoT communication with PC. The IoT-tool can be used to tune the parameters of Simulink control system of uploaded to Raspberry Pi and receive the data from simulations remotely from PC [8].

The primary purpose of this study is to design a framework for a light SBC based HIL test setup to enable easy development of control systems for semi-active hydraulic damping. The designed framework could prove to be beneficial in several fields. Employing cost-effective and relatively easy to use SCBs, a simple, modular control system with IoT capabilities can be built for a test bench to test and validate suspensions systems. The framework would also ease the implementation of semi-active suspensions, turning passive suspension systems into more efficient ones. It would improve the vehicle dynamics research, offering an easy and cost-effective way to obtain more accurate simulations results thanks to the hardware-software integration.

System Description

An HIL hydraulic test bench for examining the characteristics of suspension systems was designed. The HIL system is presented in Figure 1. In the test bench, a hydraulic actuator was coupled with a hydraulic damper to mimic a suspension system. A Simulink model with two control systems was created to control the hydraulic actuator and to adjust the damping coefficient. In the actuator control system, a simulated output signal, a road profile was generated and given as input for the hydraulic actuator. The damping control system controls the setting of a proportional valve connected to the damper in order to obtain the desired damping force. The Simulink model is uploaded from PC to RPi to run the control system standalone.

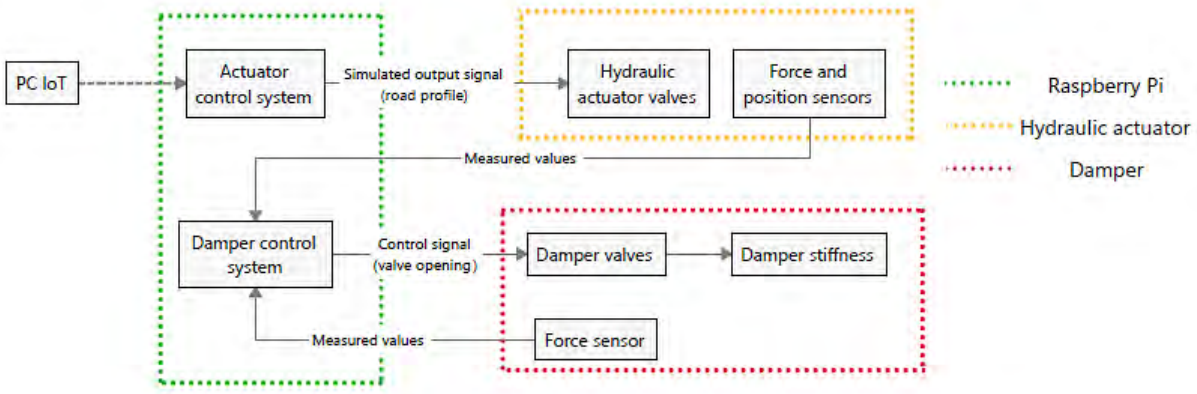

Figure 1 A simplified schematic presenting the working principle of the HIL system

The Hydraulic Test Bench. The hydraulic test bench consists of the following main components: the actuator, the damper and sensors. The test bench has two separate hydraulic circuits for the actuator and the damper. The hydraulic circuits of the test bench are shown in Figure 2.

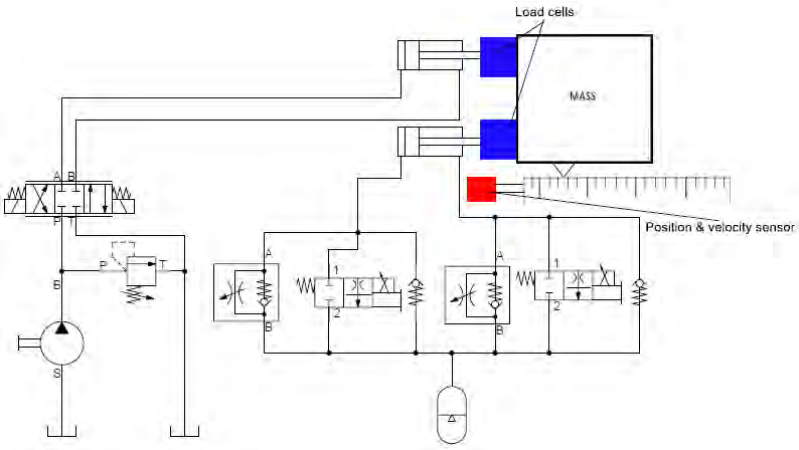

Figure 2 A schematic presenting the complete hydraulic circuit and sensor

The actuator is a hydraulic cylinder which allows to generate a wide range of input so that the semi-active damping system can be tested in different road conditions. The actuator is in an open loop circuit with a fixed-pressure pump. The movement of the actuator is controlled actively by adjusting the servo solenoid directional control valve with the output of a simulation generated in the RPi.

The damper is a double acting single rod cylinder. The damper system is a closed loop circuit, pressurized with an accumulator. Both sides of the damper have a manually adjustable flow control valve, a proportional control solenoid valve and fixed pressure check valve. The manually adjustable flow control valves enable the pressure range in the damper circuit to be manually adjusted. The proportional flow control valves allow active control over the flow through the circuit. The fixed check valves limit the maximum pressure in the damper.

As seen in Figure 2, the test bench has three sensors: two load cells and a position-velocity sensor. The load cells are attached to the cylinder rods and they measure the forces in both cylinders individually. A magnetostrictive linear sensor, with position and velocity outputs, is placed beside the damper to measure the position and velocity of the moving mass.

Setting up Real-Time System. The SBC chosen for this research to run Simulink control system model was Raspberry Pi 3 B+ due to its cost-efficiency, accessibility and compatibility with MATLAB-tools. In a recent research, the RPi model 3B was used for validation of the SBC running real-time simulations standalone [7].

The RPi model was missing analogue to digital converter (ADC), thus a 10-bit ADC hat was installed on the RPi board. In addition, the input and output signals of the RPi GPIO-pins have an operating voltage range of 0-3.3 V, while the voltage ranges for all the proportional valves and sensors are -10 V to +10 V. Thus, operational amplifier (OP-amp) circuits are required for converting signals in both directions. Since the proportional valves of the damper and the hydraulic actuator are controlled with PWM voltage, control shields were used for controlling the valves. A simplified schematic of the signal processing circuit is displayed in Figure 3.

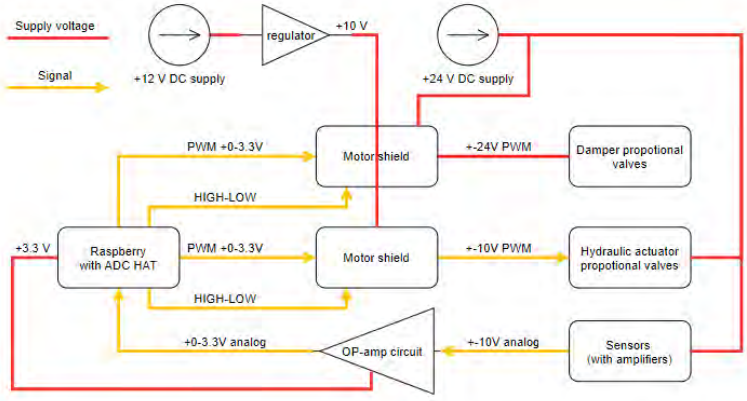

Figure 3 The signal processing circuit presenting the needed voltages for each component

Since the signal from the sensor circuits are bipolar, a regular non-inverting OP-amp for scaling the amplitude of the signal is not sufficient for converting the signal to unipolar. Thus, a level shifter OP-amp circuit had to be designed for the conversion. The solution was to connect an offset voltage source to the ground. The electrical schematic of the level shifter OP-amp circuit can be seen from Figure 4.

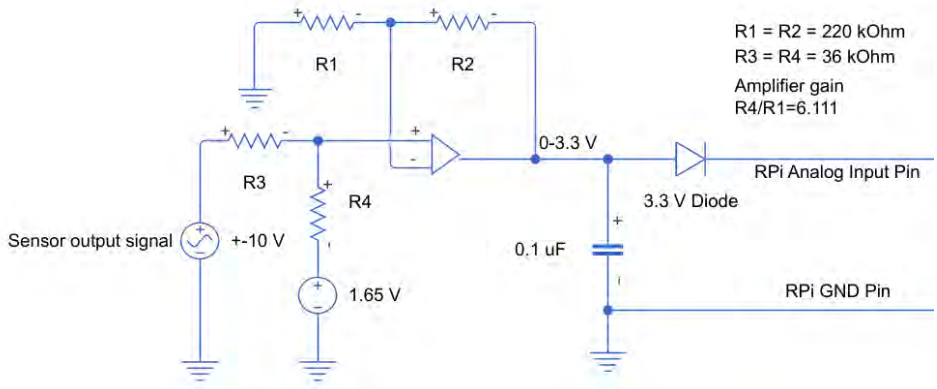

Figure 4 The circuit diagram for the designed non-inverting OP-amp level shifter

Simulink support pack installed on RPi enabled the control of the RPi board I/O pins with Simulink blocks. The Simulink model was uploaded to the Raspberry Pi from PC via IoT communication. Another useful capability of the IoT-tool was the ability to tune parameters of Simulink model live PC when the algorithm is running on the RPi.

Modeling the Real-Time Control System. A Simulink model, introduced in Figure 5, consisting of two control models was developed. The first one (green), was used to simulate the road profile and to control the actuator, the second one (blue), controlled the damping coefficient and so the damping force. The Simulink model was uploaded on the SBC, which worked as the system control unit.

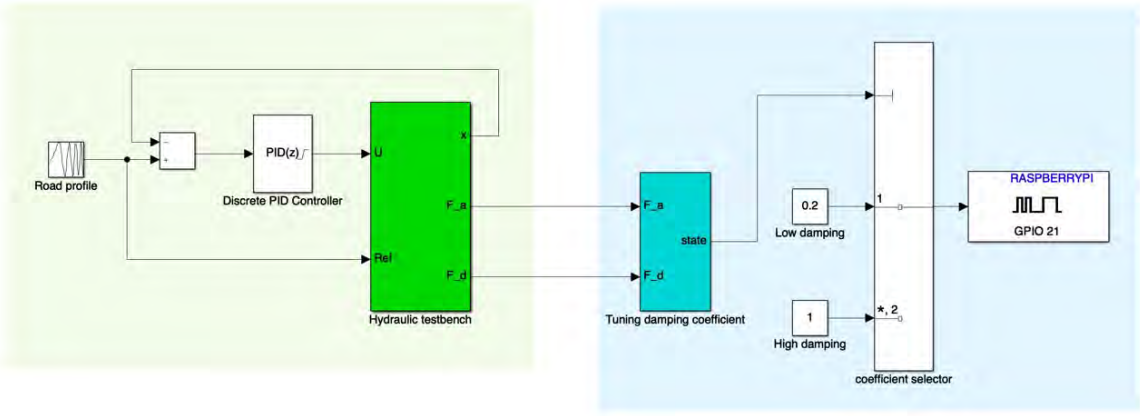

Figure 5 The Simulink model consisting of the road profile generator model (in green) and the control model (in blue)

The first control model simulates the desired road profile employed to test the examined suspension system through the movement of a hydraulic cylinder, the actuator. In the developed control model, the digital PWM signal representing the road profile, in this case a chirp signal, was properly elaborated and employed to move the actuator piston by controlling the input pressure of the actuator. In the green subsystem, the sensor data, which would be used both by the control systems and during the analysis of the suspension system, is collected and postprocessed. The control system included a PID feedback loop which guarantees that the position profile of the actuator mirrors the generated profile.

The second control model sets the proportional valve connected to the hydraulic damper in order to reach the desired damping force. To design the damper model, a simple model of a suspension system, presented in Figure 6, was developed.

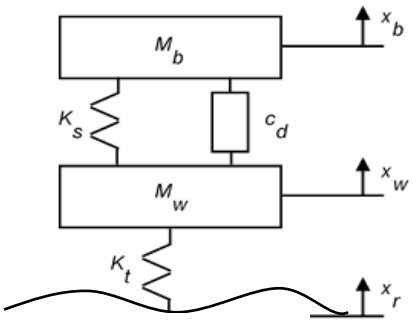

Figure 6 Suspension system sketch

The variables and parameters used in the systems are:

- Mass (M_b), position (x_b), velocity ($\dot{x}_b$) and acceleration ($\ddot{x}_b$) of the sprung mass (body);
- Mass (M_w), position (x_w), velocity ($\dot{x}_w$) and acceleration ($\ddot{x}_w$) of the unsprung mass (wheel);
- Road position (x_r)
- Spring stiffness (k_s) and tire stiffness (k_t);
- Damping coefficient (c_d).

According to dynamic analysis, the governing equation of a suspension system are:

$$M_b\ddot{x}_b = -k_s(x_b - x_w) - f_d \tag{1}$$

$$M_w\ddot{x}_w = k_s(x_b - x_w) - k_t(x_w - x_r) + f_d \tag{2}$$

where the force f_d from the damping device is given by:

$$f_d = C_d(\dot{x}_b - \dot{x}_w) \quad \text{for passive suspensions} \tag{3}$$

$$f_d = c_d(\dot{x}_b - \dot{x}_w) \quad \text{for semi-active suspensions} \tag{4}$$

In particular, in semi-active hydraulic suspensions the damping coefficient, c_d, depends on the opening of electro-proportional valves which regulate the inlet and outlet flow in the damper chambers. Skyhook control strategy was chosen to control the valves opening. The damping factor switches between high and low damping coefficient according to the velocity of the sprung mass and the unsprung mass by employing the logical rule, implemented in the blue subsystem in Figure 5:

$$c_d = \begin{cases} c_{max} & if\ \dot{x}_b(\dot{x}_b - \dot{x}_w) \geq 0 \\ c_{min} & else\ \dot{x}_b(\dot{x}_b - \dot{x}_w) < 0 \end{cases} \tag{5}$$

Results

The designed framework for the HIL test setup was validated by prototyping and testing the individual parts of the test setup. A test Simulink model was successfully uploaded to RPi from PC when both devices were connected under the same Wi-Fi. The models ran on RPi standalone without any complications. In addition, parameters of the Simulink model could be changed during simulation test runs. The hydraulic test bench and the control signal processing circuits were also validated by driving the hydraulic actuator with test Simulink models running on the RPi.

Finally, the level shifter OP-amp circuit was tested with a load cell circuit of the test bench. The functionality of the OP-amp circuit was successfully validated, but there was an issue with accuracy of received sensor data. The resolution of the sensor circuits of the test bench were 16-bit. In order to

run the RPi board in real-time, serial peripheral interface (SPI) communication must be used [7]. However, the availability of 16-bit SPI ADC modules with sufficient number of channels was limited. Thus, the 10-bit SPI ADC hat was acquired for the RPi board which dramatically decreased resolution of the sensor data.

Discussion

The SBC used in this research, Raspberry Pi 3B+, showed to have considerable limitations regarding the control and signal processing capabilities. The PWM output range and the analog input range, both being from 0 V to 3.3 V, pose challenges in the control system since industrial type sensors typically have an analog output range of 0 V to 10 V or -10 V to +10 V. Therefore, scaling the sensor output signal voltage range down to 0 V to 3.3 V results in larger error in given sensor data, making the system more sensitive to noise. Also, hand-soldered circuit boards for scaling the signal may be prone for disturbances. Therefore, using a more sophisticated SBC, namely industrial versions of RPi could be justified since they offer more flexibility regarding the PWM and analog input ranges.

Utilizing an industrial RPi could result in a more simple and robust system, less prone for external signal errors, and it could provide better compatibility with 16-bit sensors. The control shields for the proportional valves and the signal processing circuits for the sensors would be replaced with one or two ready-made modules, depending on the manufacturer. However, since the main driver is still an RPi, the modules would still scale the voltage ranges down to 0 V to 3.3 V, so the error might still be significant. Furthermore, one of the key features of the presented system is cost efficiency. The control system was built with minimal use of expensive electrical components. The price of an industrial RPi is typically multiple times the price of a basic one and with additional modules the price range for the control system rises from some tens of euros to hundreds of euros [9].

Further research is required to validate the real-time capabilities of SBC running the control system model HIL simulations on the hydraulic testbench. Also, the capabilities of other industrial control applications in HIL simulations should be researched to compare SBC solutions with existing solutions.

References

[1] El-Demerdash, Samir. (2002). Improvement of Trucks Ride Dynamics Using a Hydraulic Semi-Active Suspension System. SAE Technical Papers.

[2] Bhise, Ankita & Desai, Rutuja & Yerrawar, Rahul & Mitra, Anirban & Arakerimath, Rachayya. (2016). Comparison Between Passive And Semi-Active Suspension System Using Matlab/Simulink. IOSR Journal of Mechanical and Civil Engineering. 13. 01-06. 10.9790/1684

[3] Zhang, Ze & Karimi, Hamid Reza & Huang, Hai & Robbersmyr, Kjell. (2014). Vibration Control of a Semiactive Vehicle Suspension System Based on Extended State Observer Techniques. Journal of Applied Mathematics. 2014. 1-10.

[4] Wu, J & Lin, Chih-Jer & Kuo, K. (2008). A Study of Semi-Active Vibration Control for Vehicle Suspension System Using an Adjustable Shock Absorber. Journal of Low Frequency Noise Vibration and Active Control. 27. 219-235.

[5] W. E. Misselhorn, N. J. Theron, and P. S. Els, 'Investigation of hardware-in-the-loop for use in suspension development'. Veh. Syst. Dyn.vol. 44. no. 1.pp. 65–81. 2006.

[6] M. K. Kwak, J. H. Lee, D. H. Yang, and W. H. You, 'Hardware-in-the-loop simulation experiment for semi-active vibration control of lateral vibrations of railway vehicle by magneto-rheological fluid damper'. Veh. Syst. Dyn.vol. 52. no. 7.pp. 891–908. 2014.

[7] Walter, J., Fakih, M. and Grüttner, K., 2014, January. Hardware-based real-time simulation on the raspberry pi. In *2nd. Workshop on Highperformance and Real-time Embedded Systems*.

[8] MATLAB website, Simulink support for Raspberry PI.

[9] Kunbus Revolution Pi website, shop.

Newtonian Telescope Design for Stand-off Laser Induced Breakdown Spectroscopy

Jonas Mård[1, a *], Verneri Vilmi[1,b], Jonas Rintanen[1,c], Lasse Kangas[2,d], Ilkka Laine[2,e], Panu Kiviluoma[1,f] and Petri Kuosmanen[1,g]

[1]Department of Mechanical Engineering, Aalto University, Finland

[2] Civil and Environmental Engineering, Aalto University, Finland

[a]jonas.mard@aalto.fi, [b]verneri.vilmi@aalto.fi, [c]jonas.rintanen@aalto.fi, [d]lasse.kangas@aalto.fi, [e]ilkka.laine@aalto.fi, [f]panu.kiviluoma@aalto.fi, [g]petri.kuosmanen@aalto.fi

Keywords: LIBS, Stand-off, lens, mirror, ablation, laser, plasma

Abstract

Laser induced breakdown spectroscopy (LIBS) works by shooting laser light onto an optical system that initially expands the beam through an expanding lens and then focuses it on the sample through a focusing lens. Focusing the laser on the sample creates a plasma emitting light. This light is then focused on an optical fiber, through a light gathering optical system, which is connected to a spectrometer, where the results can be analyzed. In this research a design of a stand-off LIBS device is introduced.

This research addresses a system that scans the environment, which means that the target distances vary. The system's key components are a laser, lenses and mirrors to allow adjustments of the beam, to achieve ablation in the target sample, and the collection of emitted light from it. The importance of choosing the right components is significant in such optical setups where precision is of high priority.

The research addresses a way to design a system that works as effectively as possible and gives high quality results regarding chemical composition of target material. The device is based on a Newtonian telescope model, whereas the target is to fit most of the optical components on the same optical axis. The results show that optically, such a setup is possible for a LIBS device. Results also show that the design of such a device allows parts to be made by additive manufacturing, as long as the optics are adjustable to maintain the precision.

LIBS is a growing technology which can be used for many applications. There are still some limitations to the technology such as coatings of mirrors and lenses to allow wider wavelengths to pass through or reflect.

Introduction

Laser induced breakdown spectroscopy (LIBS) is not a new technology, but it can still be seen used in a variety of different applications. Most notable one being the ChemCam which is an integrated module on the Mars Science Laboratory Rover Curiosity. ChemCams purpose is to understand the chemical composition of rocks, minerals and soil on Mars using LIBS technology [1]. Another notable use of this technology comes from the U.S military that uses LIBS to detect explosives [2].

LIBS works by shooting laser light onto an optical system that initially expands the beam through an expanding lens and then focuses it on the sample through a focusing lens. Focusing the laser on the sample creates a plasma emitting light. This light is then focused on an optical fiber, through a light gathering optical system, which is connected to a spectrometer, where the results can be analyzed.

LIBS is a very useful technology to use for analyzing the chemical composition of different materials. LIBS as a technology has been around for a while, but there are lots of different variants and applications of the technology.

In stand-off LIBS the range to the sample varies, which makes the device more complex since the position of the lenses and gathering optical fiber must be controlled so that the ablation point, and the gathering point of light stays optimal. A unique feature of LIBS is that samples can be detected remotely, which can be a valuable tool for determining different environmental samples [3].

Receiving accurate data of the chemical compositions of rocks and minerals that are present in the mine, with the help of a stand-off LIBS system, is a lucrative option for the mining sector. Using a stand-off LIBS system is safe and gives accurate data of the structure and contents of the mine.

The project is based on the Laine (2019) stand-off LIBS prototype, where optics related issues like focusing and energy reduction needed for ablation are to be improved. The key aspect to be improved is the focusing optics of the system. [4] The main challenge to tackle is that the device must collect plasma emission in a varying wavelength range, and that the device is able to work in varying distances. This means that the optics of the system must be controlled, in relation to distance to the sample. Béatrice Sallé et al. tested different setups in a laboratory environment that can be used to collect data at distances between 3 - 12 m [5].

Gabriela Vítková et al. uses a three lens Galilean telescope to focus the laser and the collection is done with a Newtonian telescope equipped with a mirror which reflects the light into an optical fiber [6]. The ChemCam is able to collect data from 1 - 7 m distance by moving the secondary mirror which enables the laser to be focused onto different distances [1].

The goal of this project is to improve the current optical setup which is not able to gather the desired amount of UV light and requires modifications. In this research the aim is to create an optical setup for a standoff LIBS system which can gather plasma emitting light from 200 - 950 nm. The optical setup must be able to gather the plasma emitting light from distances of 3 - 10 m.

Methods

The goal of the prototype was to get most of the lenses and mirrors to the same optical axis. In Fig. 1 we can see an illustration of the system with light trajectory. The idea for the concept was based on the Newtonian telescope.

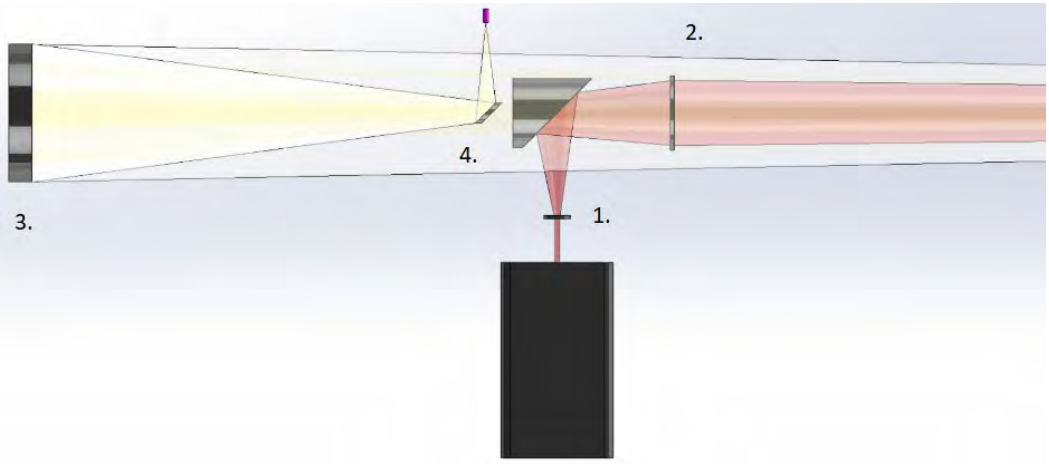

Fig. 1 The concept of the prototype with illustration of light behavior

Optics. The laser was focused with a N-SF11 plano-concave lens (1) which breaks the laser light. The broken laser light was directed to a 45° laser mirror from which the light went through a N-BK7 plano-convex lens (2) which focuses the laser light on to the wall. For the gathering optics a self-made Newtonian telescope was used. The mirrors used for the telescope were UV enhanced aluminum mirrors for both the primary (3) and secondary (4) mirrors. The primary mirror is a spherical mirror that focuses the gathered light to one point which can be directed into the optical fiber. The secondary mirror is an elliptical mirror installed in a 45° angle to the primary mirror which was used for turning the gathered light 90° into the optical fiber. Focal point and sizes of mirrors and lenses can be found in table 1.

Table 1 Mirrors and lenses used for the LIBS device. f = focal length.

	Components	Specifications
1.	N-SF11 plano-concave lens	f = -15.0 [mm], Ø12.5 [mm]
2.	N-BK7 plano-convex lens	f = 200.0 [mm], Ø75.0 [mm]
3.	Primary mirror	f = 609.6 [mm], Ø150 [mm]
4.	Secondary mirror	Minor axis: 22.23 [mm], Major axis: 31.42[mm]

Prototyping. Some parts we had to customize ourselves to our specific needs, such as the telescope with necessary parts. The telescope frame and holders for the mirrors were 3D printed from ABS. These 3D printed parts were designed in a way that allowed adjustments of the positions and angles to achieve required precision for the system.

Results

Final 3D CAD assembly of the prototype (Fig. 3) was made in order to prove that the selected optical equipment can be fitted onto the given breadboard. Some parts were 3D printed to see if it was a viable option for manufacturing components for this kind of precise optical system.

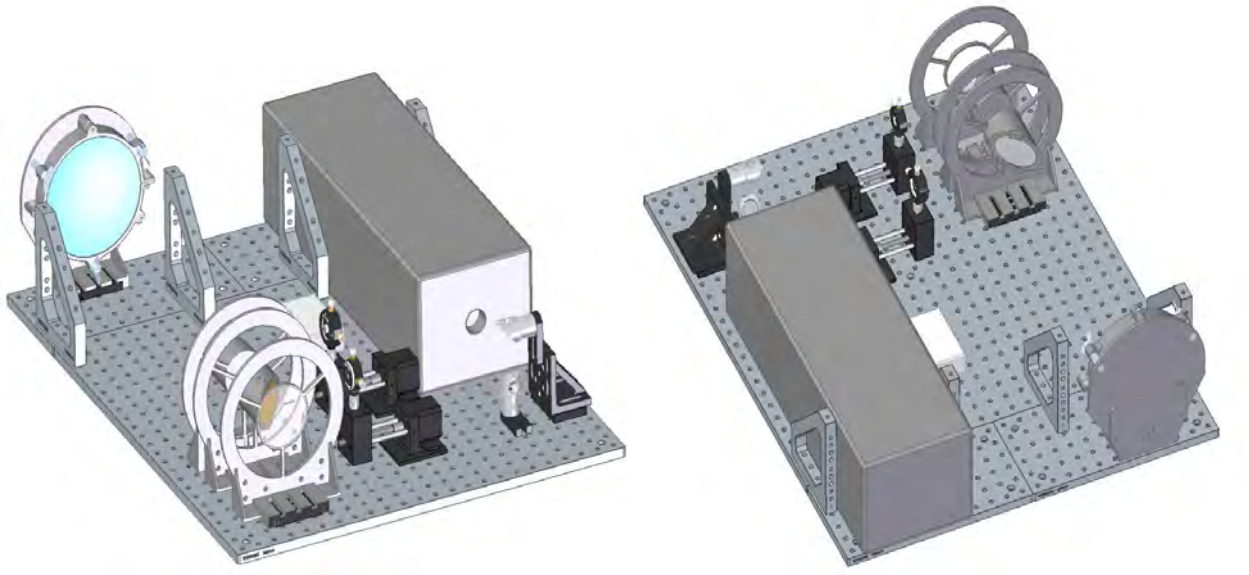

Fig. 3 Isometric view of the final LIBS setup with all the lenses and moving components visible

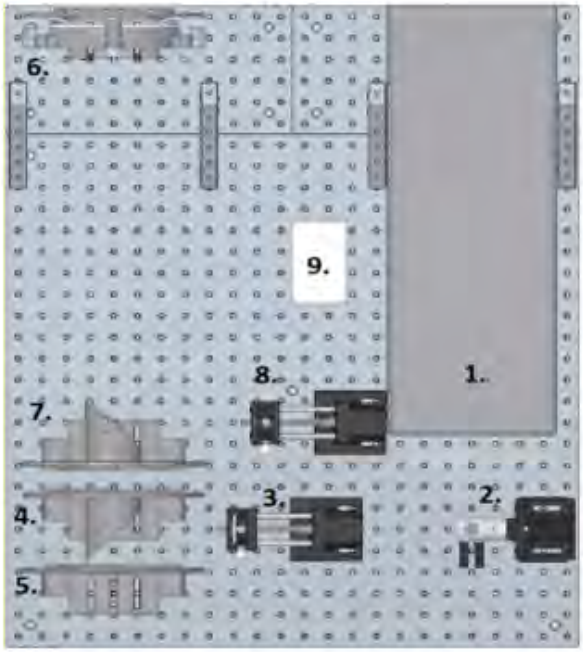

1	Laser (Quantel Q-Smart 450, 1064 nm)
2	2 x 45 ° mirrors
3	Linear stepper actuator with plano-concave lens
4	45 ° gold plated mirror
5	Plano-convex lens
6	Primary mirror
7	Secondary mirror 45°
8	Linear stepper actuator with optical fiber
9	Spectrometer (BWTEK Exemplar LS)

Fig. 4 View from above of the LIBS setup

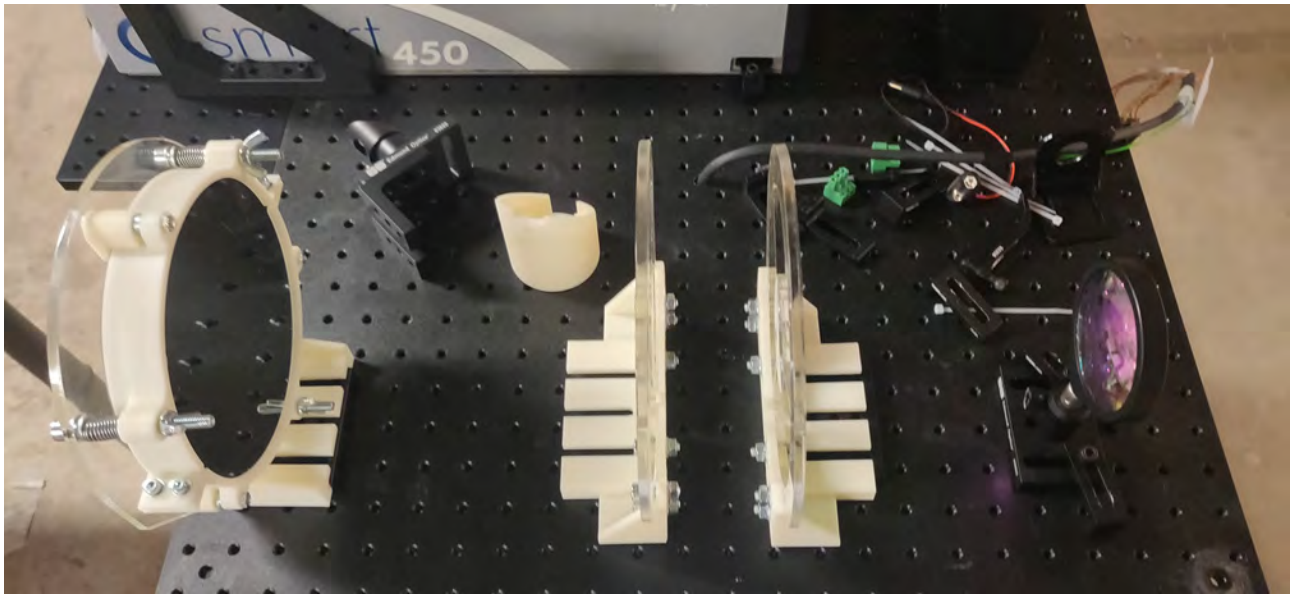

Fig. 5 3D printed prototypes of the primary, secondary and laser mirror holders

Design aims to maximize the utilized area of the primary mirror by keeping the area constructing the passage of the returning light at a minimum. By using this setup, over 50 % and up to 60 % of the primary mirror reflecting area gathers returning light from 3 to 10 m distances.

Tests. This prototype can be tested to prove the concept of this kind of Newtonian telescope design. Aim of these tests are to determine the minimum laser power required for a successful spectrometry graph. Testing setup is going to have multiple ranges from 3 to 10 meters where a test sample can be reliably and reproducibly shot with the laser pulse using several different power levels of the laser. Then from the collected data from the spectrometer it can be seen what the minimum power level is to get a sufficient amount of plasma formation.

Secondly, the ability to scan and adapt to the varying distance without affecting the data will be confirmed by a test setup. For this test, a uniform plane with a homogenous material is going to be placed in front of the laser. After this a LIBS scanning will be performed, and after this the gathered data will be analyzed to find if the device is able to perform a scanning with stable performance and without producing artefacts in the data.

Controllers and Calibration. Stand-off LIBS means that the range varies, and the device is scanning the environment, which requires different controls, adjustments, and other techniques for calibration. For measuring distance, a laser rangefinder will be used, which measures the distance from the focusing lens to the sample. For achieving optimal ablation-point, the device will be calibrated by adjusting the negative laser expanding lens, and light receiving optical fiber linearly with stepper motors, to adjust the focus. Moreover, the optimal point is achieved by including the sound level, distance measurement from the rangefinder and light intensity in optical fiber, whereas maximum noise gives the best ablation effect. Measuring the sound level of the ablation effect will be captured with a microphone. The stepper motors for the negative lens uses Arduino based control to find the optimal position for highest sound intensity.

Before scanning with the device, the calibration must be initiated. A test sample will be set at a distance, where both the rangefinder and laser beam hit the sample. A calibration point is then saved with information about distance of the rangefinder, and microphone reading. Furthermore, the LIBS is then turned on and the autofocus system drives the negative lens to the position with highest sound intensity, and the optical fiber drives to the position with highest light intensity. This calibration is done for multiple distances, and when finished, target positions for the steppers are calculated from the calibration curves.

The primary mirror in the Newtonian telescope is manually adjustable by adjusting three points in the frame connected to the mirror. The optimal position of the mirror can be sought, by using a laser pointer as reference light to mimic the light emitting from the plasma in the calibration stage.

Discussion

Design that is presented in this research is a seemingly improved version of the LIBS scanner Laine built and described in his study [4]. Before making a definite claim that the prototype solves the problems, regarding the focusing and the amount of the gathered returning light, that Laine's device struggled with, a working prototype should be built and tested. The usable primary mirror area is 5.9x larger. This then allows a lower laser power and higher pulse frequency. Lower power makes the device safer to the user and lower the energy consumption. Higher pulse frequency saves time as the scanning operation can be concluded faster. Next steps in the research and development are to make the system more reliable, mobile and robust.

References

[1] Washington University in St. Louis. (2019) Chemistry Camera (ChemCam). Available at https://an.rsl.wustl.edu/mer/help/Content/About%20the%20mission/MSL/Instruments/ChemCam.htm. [Accessed 23.1.2020]

[2] Applied photonics. (2012). Stand-Off LIBS Projects - Past & Present. Available at http://www.appliedphotonics.co.uk/products_services/gen4_5.htm [Accessed 23.1.2020]

[3] M. Tamboli et al. (2016). Development of a Stand-off Laser Induced Breakdown Spectroscopy (ST-LIBS) system for the analysis of complex matrices, Journal of Instrumentation, IOP Publishing, Vol 11, available at doi:10.1088/1748-0221/11/08/P08021[Accessed 23.1.2020]

[4] Ilkka Laine (2019). Scanning laser-induced breakdown spectrometer for mine walls. Available at http://urn.fi/URN:NBN:fi:aalto-201906233970 [Accessed 23.1.2020]

[5] Béatrice Sallé et al. (2004) Laser-Induced Breakdown Spectroscopy for Mars surface analysis: capabilities at stand-off distances and detection of chlorine and sulfur elements, Spectrochimica Acta Part B: Atomic Spectroscopy, Vol 59, Issue 9, pp 1413-1422, Available at https://doi.org/10.1016/j.sab.2004.06.006. [Accessed 23.1.2020]

[6] Gabriela Vítková et al. (2012). Fast identification of biominerals by means of stand-off laser-induced breakdown spectroscopy using linear discriminant analysis and artificial neural networks, Spectrochimica Acta Part B: Atomic Spectroscopy,Vol 73, pp 1-6. Available at https://doi.org/10.1016/j.sab.2012.05.010. [Accessed 23.1.2020]

Simulation and Testing of Temperature Behavior in Flat Type Linear Motor Carrier

Robert Hermansson[a], Muhammad Usman[b], Mehrdad Khodayari[c], Kimmo Hirvonen[d], Panu Kiviluoma[e] and Petri Kuosmanen[f]

Department of Mechanical Engineering, Aalto University, Finland

[a]robert.hermansson@aalto.fi, [b]muhammad.3.usman@aalto.fi, [c]Mehrdad.khodayari@aalto.fi, [d]kimmo.hirvonen@aalto.fi, [e]panu.kiviluoma@aalto.fi, [f]petri.kuosmanen@aalto.fi

Keywords: Heat Transfer Analysis, FEM-analysis, Electric losses

Abstract

The common problem with linear motors is the heat production which limits the performance and reduce the accuracy of the motor. In this research, temperature behaviour of Flat Type Linear Motor Carrier is simulated and verified with actual temperature measurements, and the accuracy of the applied methodology is evaluated. Simulation consists of two parts: (1) Estimation of power losses in heat generation, and (2) steady state heat transfer analysis at estimated power losses. Electric power losses are calculated based on the power loss equations, given in motor documentation. Heat transfer analysis is carried out with calculated power losses, at moderate convection coefficient of the air. Simulations and experimental evaluation prove that temperature behaviour of the linear motor carrier can be estimated precisely using this methodology.

Introduction

As a demand of speed and accuracy in modern manufacturing, linear motors are nowadays used in many high-performance machine tools and production machines. Linear motors offer high power density in compact design. Because of the direct drive mechanism, they can produce fast and precise movements with high forces without any backlash. There are no wearing drive components in the main actuator, which could break down or affect the accuracy, making the linear motors durable and reliable linear actuators. [1] The working principle of a permanent magnet linear motor (PMLM) is similar to a normal rotary servo motor. A Flat type permanent magnet linear motor consist of the coil section, called the primary section, and the permanent magnet track, called the secondary section. The primary is attached to the linear motor carrier, which moves along the secondary track. The motion force is generated by applying varying current to the primary section coils, which creates a magnetic field around the coils. This magnetic field creates a magnetic force between the primary and secondary section, making the carrier to move along the track. The motor speed is controlled by changing the frequency of the current, and the force is controlled with the level of the current. [2]

The major drawback of linear motors is the heat generated in the primary coils due resistance at high currents, which limits the performance and accuracy of the motor. Because the primary section is attached to the motor carrier, the heat conducts straight to the working area causing unwanted heat stress and deformation. Two studies can be found to investigate the deformation of the linear motor carriage due to the temperature [3] [4] using FEM-analysis as a primary tool. One of them [4] assumed the thermal deformation can be 70% of the total positioning error. The coils and other parts of the motor can also suffer significant damage due to the excessive heat, so the temperature behavior must always be considered when designing the working cycles. There is also research done on the effect of the water-cooling system used in the linear motor [5], and the effect of the different permanent magnet rotor configurations on temperature [6].

In this research we are testing and simulating the temperature behavior of Siemens 1FN3-3050 linear motor [1], which is a PMLM controller with Sinumerik 840d sl CNC-controller [7]. We are

developing a simulation model/method to analyze the temperature behavior of a flat type linear motor using Solidworks´ thermal simulation-analysis along with MATLAB Simulink. We are also using experimental tests to study the temperature behavior in real life by applying external load to the motor and running it over continuous duty-cycle while measuring the temperature on the top of the carriage. The experimental results and simulation results are compared to verify the accuracy of simulation.

Methodology

For the purposes of this study, the carriage section of Siemens 1FN3-3050 linear motor was modified in a way, that different loads can be attached to it. Two different temperature sensors were used to obtain the temperature values, close to the top surface of the coil section at two different locations. An intermittent cycle with rapid movement was utilized to study the long-term effect of the heat generation in the coil section. Water cooling which is used for cooling the coils section was disabled so, that the heat would only be transferred to the aluminum carrier. Test drive for linear motor was implemented with 15.6 kg additional mass and motor movement cycle was done with a speed of 30000 mm/min for 150 mm with 0.2 s dwell periods between movements. This cycle was continued for 1 h 42 min.

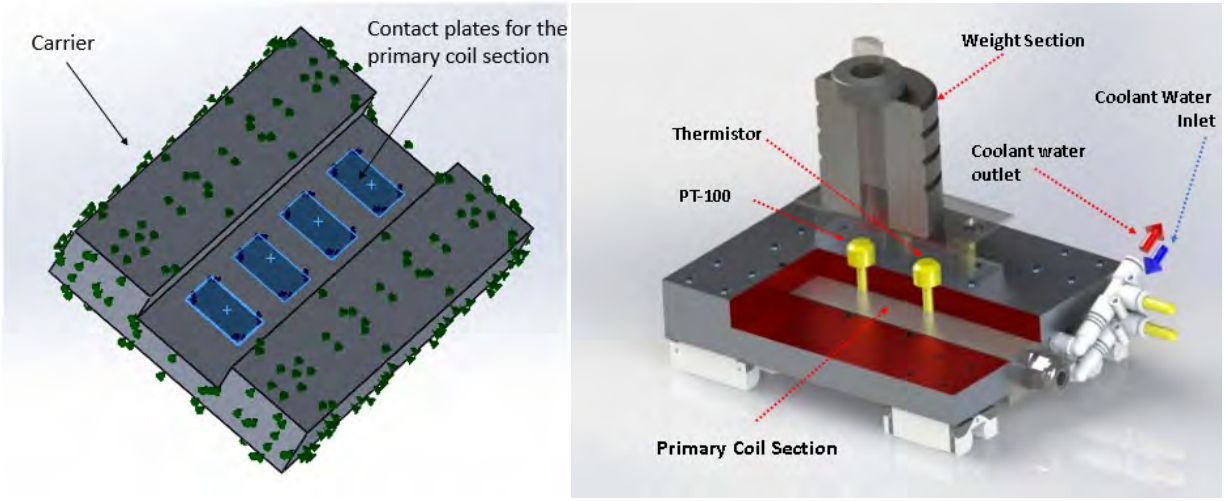

Figure 1. Empirical test setup. Carrier bottom (left side). Carrier top (right side).

To simulate the behaviour of the linear motor, a Simulink model was created. Then, heat transfer analysis in Solidworks was performed to simulate temperature distribution, depending on the power losses obtained from Simulink model. Finally, data obtained from heat analysis was compared with sensors data to validate the study.

MATLAB/Simulink Model. A simple MATLAB/Simulink model was developed based on temperature equations, coefficients and constants given in motor documentation at rated power consumption, when the motor operates at rated velocity exerting rated force, to estimate the electric power losses in heating the coils (Figure 2).

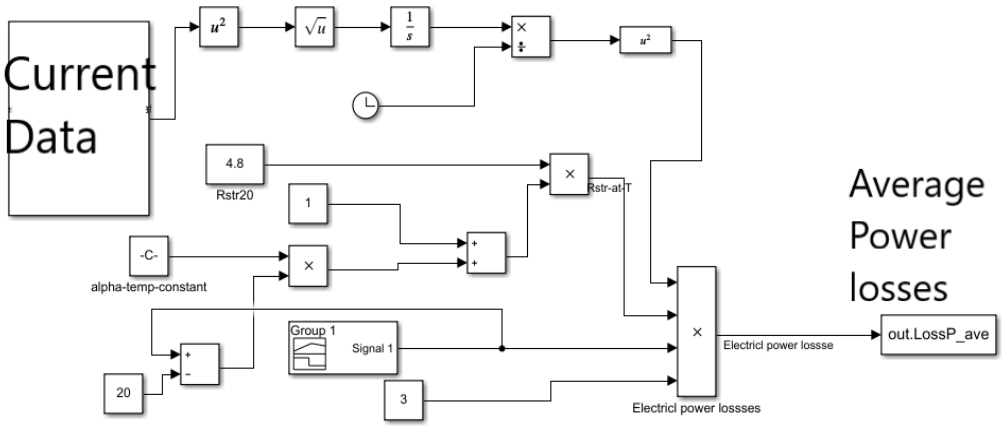

Figure 2. Simulink model for calculating heat power loss from current data obtained from Sinumerik CNC-control data trace.

For simulation of power losses into temperature, data was obtained from Sinumerik control user interface. In MATLAB/Simulink this data was accessed from a spreadsheet. Frictional and electromagnetic losses and water cooling are ignored in the Simulink model and disabled on the motor itself. The average of current data was supplied to electric losses equations to compute the average power lost in heating the coils. The average power obtained from simulation was utilized to perform Heat Transfer Analysis in Solidworks. All the graphs displayed in paper are according to simulation time and time step. The power loss was calculated using equation (1)

$$P_{V,N} = 3 \cdot R_{STR}(T_N) \cdot I_N^2 \quad (1)$$

Where $P_{V,N}$ is power loss at rated temperature T_N , rated current I_N and line resistance of the winding at a winding temperature of 20 °C, R_{STR}. The line resistance R_{STR} can be calculated for other temperatures as follows, with the temperature coefficients $\alpha = 0.00393$ 1/K for copper using equation (2)

$$R_{STR}(T) = R_{STR,20}[1 + \alpha(T - 20\ °C)] \quad (2)$$

For the sake of simplicity, it was assumed in simulation that the temperature rises linearly from 20 °C to 23 °C within 10 s, while the motor operates at rated power. The constants used in simulation are given in the Table 1.

Table 1. Constants used in Simulink modelling

Rated temperature	T_N	120 °C
Motor winding resistance at 20 °C	$R_{STR,20}$	4.8 Ω
Rated current	I_N	2.82 A
Rated Force	$_{FN}$	151 N

Heat Transfer Analysis. The heat transfer Analysis was based on the energy efficiency of the coil. The supplied electrical power from the motor driver was transformed into mechanical power and heat loss. In a steady state mode, the dissipated heat loss leads to a heat equilibrium after the motor started working in the same cycle for considerable amount of time. This was observed by means of the implemented sensors on the top of the coil section and recording their values over time. Following this logic for heat analysis, steady state analysis was performed for the carriage component. Inputs and boundary conditions for heat power and heat convection were obtained with the following methods.

Heat Power. The value for this parameter was the difference between power input from the driver and the mechanical power. Since the coil section was not in the complete contact with aluminium carriage, the CAD model was also modified as Figure 1 to comply with the real component as the way it was in contact through the aluminium contact plates presented on the left side of the Figure 1.

Convection. The convection from the part and the surrounding area plays a major role in the heat dissipation. The governing equation for convection is (3):

$$q=h(T_{air}-T_{surface}) \quad (3)$$

Where T_{air} is the ambient temperature. Since the movement of the carriage was rapid but quite short, convection coefficient of the air for the simulation was set at 11 W/m^2K which was the value associated with almost still air over a surface [8]. Also, the ambient temperature for simulation was taken as the temperature of the test day. All the important and exposed surfaces to the open air were taken as the active surfaces and included in convection.

Results

Simulink simulation. The Simulink model simulation as shown in the Figure 3, shows the average electric power losses as a function of time. The value reaches to 49.68 W at the end of the cycle. This value was also used as the heat power which is induced to the aluminum carrier in heat transfer analysis.

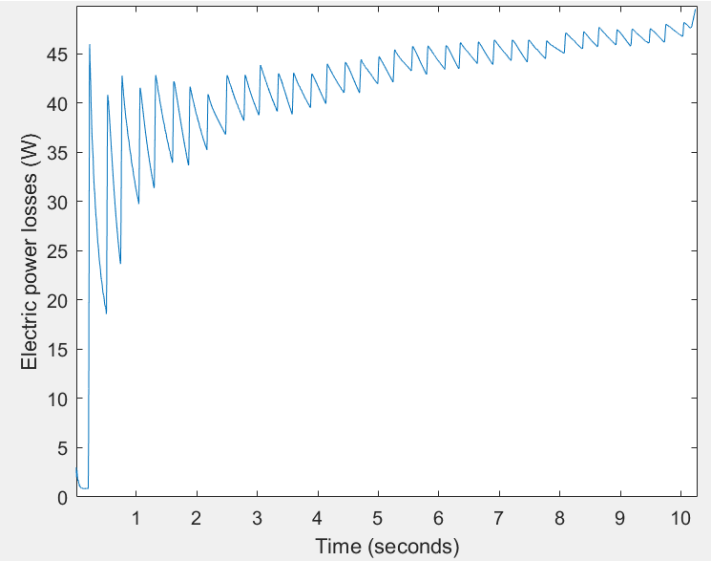

Figure 3. Electric power losses as a function from time from the Simulink simulation.

Heat Transfer Analysis in Solidworks. Heat transfer FEM-analysis in Solidworks as shown in Figure 4 and Figure 5, demonstrate the temperature distribution in aluminum part. Based on the results from the analysis, at the locations where temperature sensors are located derived values are around 57 degrees.

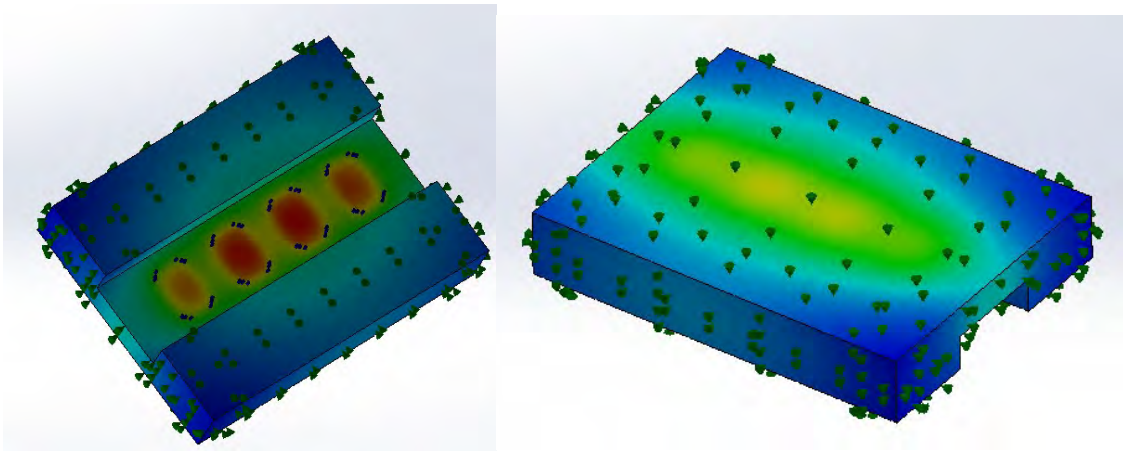

Figure 4. Steady state FEM analysis results of the carrier with top and bottom view of the carrier.

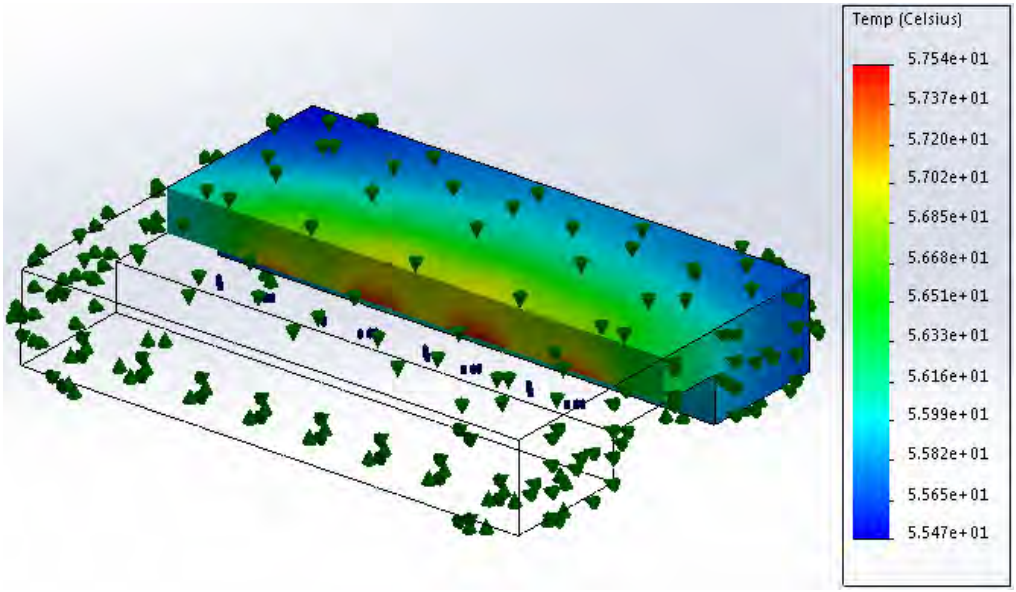

Figure 5. Steady state FEM analysis of the carrier with a temperature scale and a section view of the carrier.

Empirical tests. After running the cycle for 1 h 42 min, temperature recorded by the thermistor temperature sensor at the top of the coil section is increased from 22.6 °C to 56.9 °C (Figure 6). This value is quite close to the value obtained from the heat simulation. It can be concluded that the heat loss value from Simulink model is quite close to the real heat loss and heat simulation is showing accurate temperature distribution.

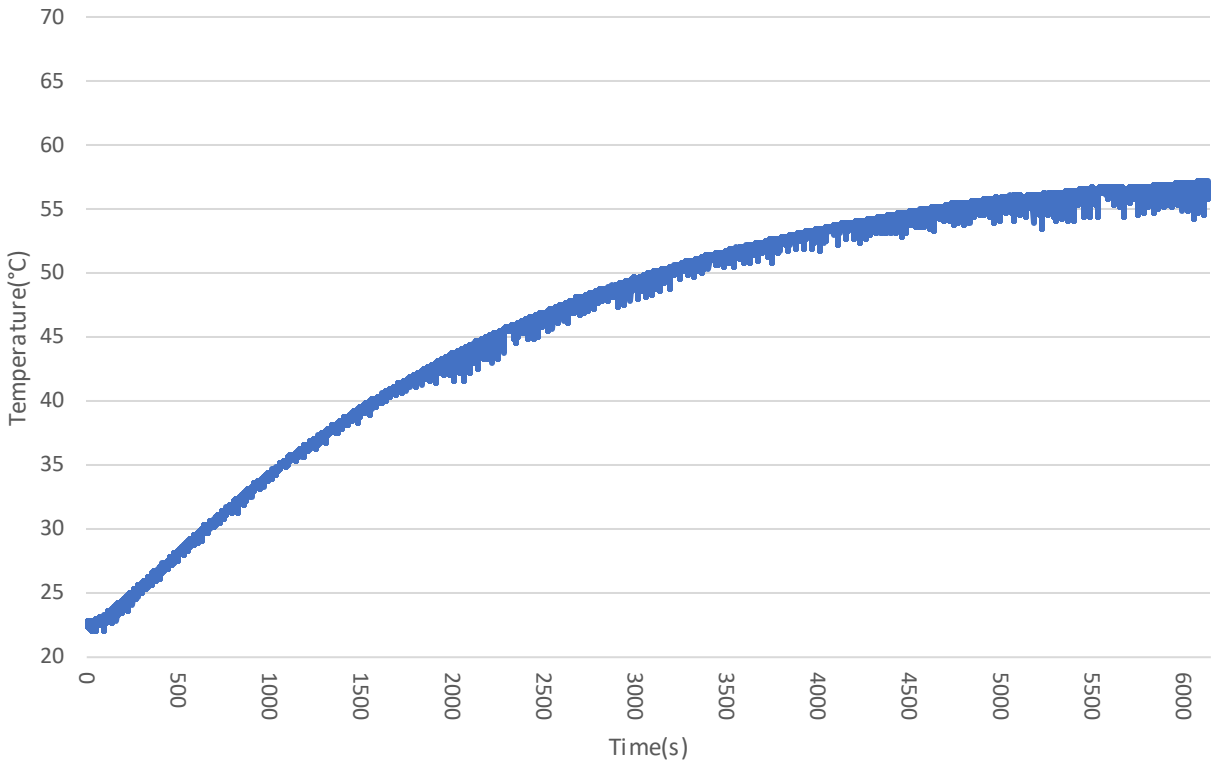

Figure 6. Actual measurement of test drive.

Discussion

The results from the simulation and empirical test are close to each other with final temperature of 57 °C. Some assumptions made for the simulation constants, like air convection from the motor carrier, have small effects of how accurate the simulation results are. To be completely sure about the accuracy of the simulation results, more tests and comparison with different kind of cycles are needed to be done. The results and methods used in this work can be used to further study the load and cycle effect on temperature in the flat type linear motors. With the same experimental setup motor could be driven with different loads and working cycles to study how they affect to the heat generation. The effect of the water-cooling system could be also studied by driving the different cycles with the water cooling on or off. The simulation model/method could be also expanded/modified to study the temperature behavior over other kind of cycles. The model can also be used as inspiration for studying performance of linear motors or the temperature behavior in other applications.

References

[1] Siemens, "SIMOTICS L-1FN3 Linear motors," [Online]. Available: https://new.siemens.com/global/en/products/drives/electric-motors/motion-control-motors/simotics-l.html.
[2] Motion Control Online, "How does a linear motor work?," 2017. [Online]. Available: https://www.motioncontrolonline.org/content-detail.cfm/Motion-Control-Tech-Papers/How-Does-a-Linear-Motor-Work/content_id/2085.
[3] De-Shau Huang, Jiye-Siang Shih, Hung-Chih Hsia & Ming-Tzer Lin, "Three-Phase Linear Motor Heat Transfer Analysis Using the Finite-Element Method," Heat Transfer Engineering, vol. 31, no. 7, pp. 617-624, 2010.
[4] J. H. Chow, Z. W. Zhong, W. Lin, L. P. Khoo, W. J. Lin and G. L. Yang;, "Investigation of thermal effect in permanent magnet linear motor stage," in 2010 11th International Conference on Control Automation Robotics & Vision, Singapore, 2010.

[5] Q. Lu, X. Zhang, Y. Chen, X. Huang, Y. Ye and Z. Q. Zhu, "Modeling and Investigation of Thermal Characteristics of a Water-Cooled Permanent-Magnet Linear Motor," IEEE Transactions on Industry Applications, vol. 51, no. 3, pp. 2086-2096, May-June 2015.
[6] M. N. a. M. Rosu, "Thermal analysis of a large permanent magnet synchronous motor for different permanent magnet rotor configurations," in IEEE International Electric Machines and Drives Conference, Cambridge, MA, USA, 2001.
[7] Siemens, "Sinumerik 840," [Online]. Available: https://new.siemens.com/global/en/products/automation/systems/cnc-sinumerik/automation-systems/sinumerik-840.html.
[8] The Engineering ToolBox, "Convective Heat Transfer," [Online]. Available: https://www.engineeringtoolbox.com/convective-heat-transfer-d_430.html.

Powder Removal Device for Metal Additive Manufacturing

Raimo Vepsäläinen[1, a*], Christian Ranta[1,b], Juho Lavio[1,c], Roy Björkstrand[1,d], Panu Kiviluoma[1,e] and Petri Kuosmanen[1,f]

[1]Department of Mechanical Engineering, Aalto University, Finland

[a]raimo.vepsalainen@aalto.fi, [b]christian.ranta@aalto.fi, [c]juho.lavio@aalto.fi, [d]roy.bjorkstrand@aalto.fi, [e]panu.kiviluoma@aalto.fi, [f]petri.kuosmanen@aalto.fi

Keywords: PBF, Powder Bed Fusion, metal 3D printing, rapid prototyping, powder removal

Abstract

Major part of metal additive manufacturing is done with powder bed-based methods. When printing parts with overhangs, support structures are needed. Metal powder trapped inside the support structures needs to be removed before detaching the part from building platform and before post-processing. Powder removal is intensive and time-consuming labour if it is done manually. Manual powder removal can also pose safety risks, such as respiratory damage. With the use of an automatic powder removal device the process can be performed without manual labour, while providing constant results and in a safe manner. In this study, a design for automatic powder removal device for metal additive manufacturing is proposed. The device is designed for research purposes with the focus in safety, simplicity and low cost. It provides a safe and simple way to perform powder removal by users with no prior experience.

Introduction

Metal additive manufacturing (AM) has been recognized as a useful way to produce complex metal parts [1]. In addition, the method offers a practical way to prototype machine parts with realistic properties. Major part of metal additive manufacturing is done with powder bed-based methods. This is a beneficial way to keep the durable structure of the metal while utilizing additive manufacturing.

Major part of AM produced parts are so complex that their dimensional control and surface integrity is degraded during the AM process. Proper heat conduction and support for overhang structures are needed. These matters form a requirement for support structures to be included in the construct [2]. During the AM process, significant amount of the powder is left into these support structures. Residual powder must be removed before post-processing the surface and before the final heat treatments [3]. This creates the need for a powder removal device [4]. A careful powder removal will help preventing the potential risks related to the use of the powder, such as damaging organs if inhaled or triggering an explosion if heated [5].

There is a low number of powder removal devices, since traditional ways are possible to use, despite being hazardous and inefficient [6]. Traditional ways mean for example removing the powder by hammering the AM build plate as it is placed upside down on a container. Hammering gets the powder moving out of the structures and then it falls to the container. Lack of cover and sealing is what makes the traditional removal process hazardous. The potential contamination risk is the most significant one. The lack of monitoring makes the method inefficient. It is impossible to confirm when all the powder is removed. Some existing powder removal devices are in industrial use, but they are expensive and not suitable for experimenting with different powder removal methods [6].

In this research, a cost-efficient AM powder removal device design with removal method experimenting possibilities is introduced. The design covers the mechanical, electrical and control design for a functional device. With the completed design and some physical prototyping, it is proposed that this type of a design is possible to be implemented in practice.

Methods

When the printing has been finished, the workpiece is left attached on the build plate as the removal device is designed for the standard sized build plate. After the powder removal process the workpiece can be removed from the building platform for post-processing. The main requirement for the device is that it can remove all the loose powder from the printed part and building platform in a specified time. To realize the operating principle of the device, the intended operating procedure is listed phase by phase. Most common post-processes include heat treatments and surface treatments. The procedure phases are as follows:

1. Operator detaches build plate from the printer.
2. Operator attaches the build plate to the base on the rotational axle of the removal device.
3. Operator closes the device and starts the removal process.
4. Device turns the workpiece around two axes. This enables all the structure cavities to open upside down for the powder to flow away.
5. Device vibrates in order to get powder to flow out.
6. Procedure enables removal of powder and when the cycle has ended, the part contains no powder in its structures.

Key components are the two axle constructions that enable the orientation changes around primary and secondary axes during the removal process, and the vibration motor which is used to get trapped powder to flow out from the support structures of the printed part. The axes can be seen in Fig. 1.

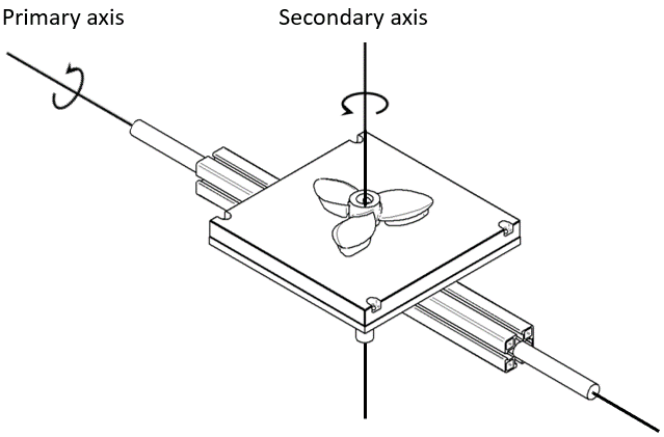

Figure 1. Rotational axes of the mechanism.

Components used to construct the powder removal device have several requirements concerning safety and torsional and vibrational stresses related to the operation of both axes and the vibration motor. As the axes are rotated, torque from the mass of the build plate and motors is applied to the stepper motors, which must be taken into account.

A vital tool during the design process was CAD (computer aided design). Feasibility of the operational principle and each modelled component were ensured in the assembly before practical realization. Development of the design and placement was an iterative process of modification and adaptation. Additive manufacturing was utilized in the production of the modelled belt drive pulleys. PLA (polylactic acid) extrusion was utilized as it offers rapid prototyping possibilities and the resources for this were easily accessible.

In order to achieve safe operation, surrounding chamber walls must be airtight to keep the hazardous metal powder from spreading into the air around the device. This is achieved by using polycarbonate panels with rubber seals all around the chamber walls. In addition, reduced air pressure inside the chamber, achieved with a fan, helps to keep air born powder inside the system.

Fig. 2 shows the main components of the device, their purpose and specifications. Rotational movement of the 3D printed part is achieved with two stepper motors, since they have suitable torque,

and they are easily and precisely controlled with a microcontroller. The horizontal primary axle movement requires more torque (~7 Nm), and therefore a 50:1 reduction gear was used along a Nema 23 sized stepper motor. The vertical secondary axle rotation will be achieved with another Nema 23 stepper motor, but without gearing.

Arduino Mega was chosen as the controller of the powder removal device. Programming was done in C, using programming libraries *LiquidCrystal* for the user interface display and *Stepper* for the stepper motors. Main focus for the program structure was simplicity and intuitive user experience.

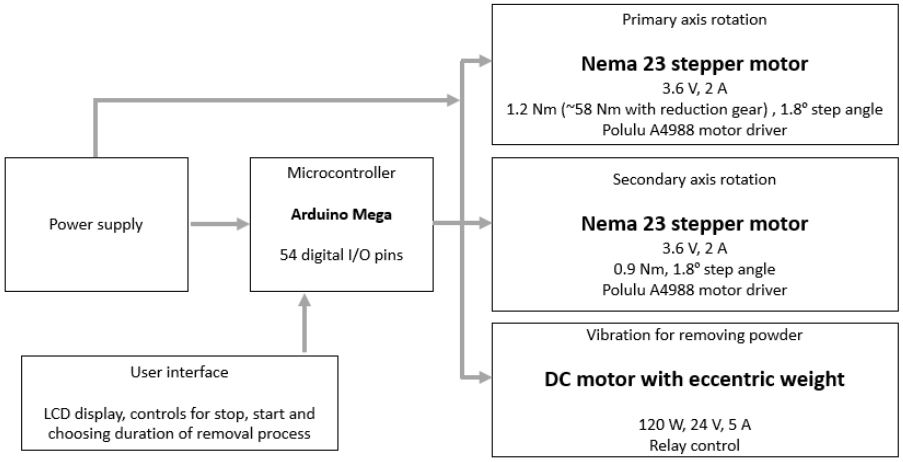

Figure 2. Simplified circuit diagram.

Results

CAD model and physical prototype of the main mechanism of the device can be seen in Fig. 3, which includes the primary and secondary axes implemented with the specified stepper motors, vibration motor and belt drive components.

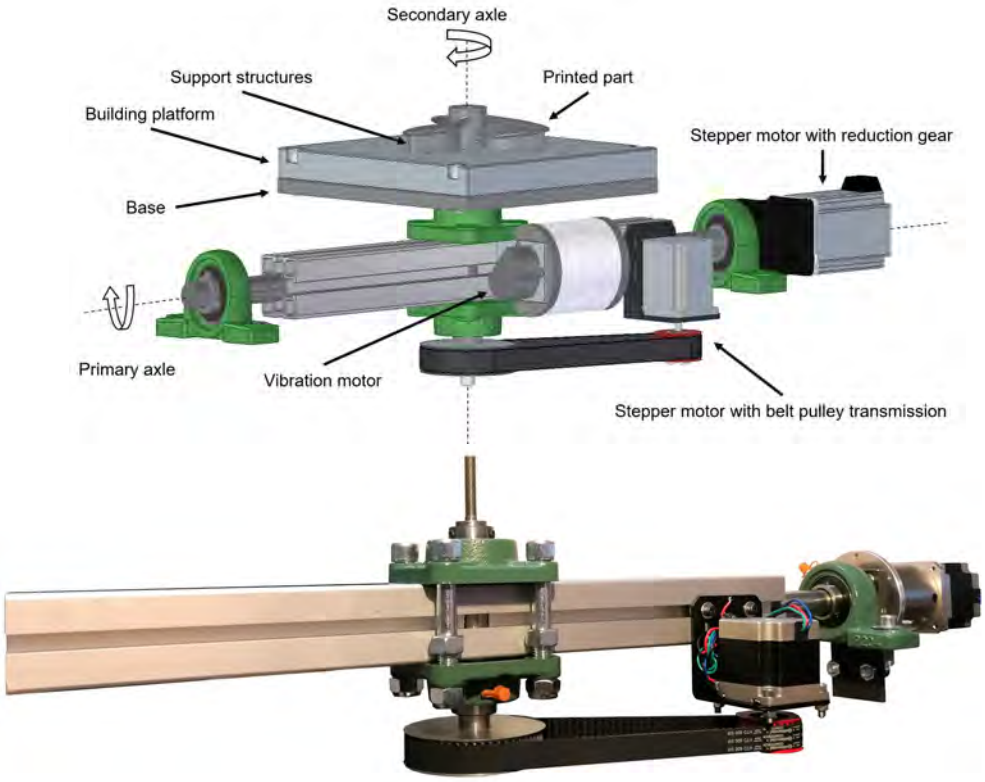

Figure 3. CAD model and physical prototype of the main mechanism.

The frame for the device was constructed mainly from aluminum T-slot profile and polycarbonate panels for easy modularity and low cost. Dampening rubber materials were used on bearing mounts and the polycarbonate panels to minimize unwanted vibrations from the vibration motor to the chamber frame. The inside chamber dimensions are 700 x 700 x 500 mm to enable easy and ergonomic installation of the build plate while allowing 360° rotation movement to take place. The chamber frame can be seen in Fig. 4.

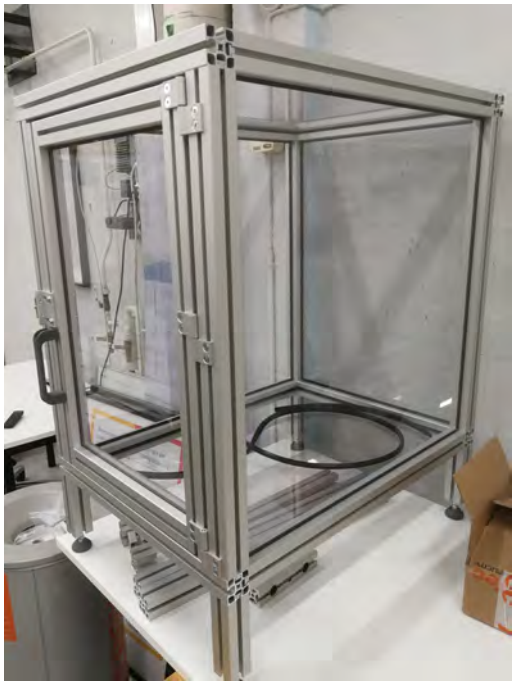

Figure 4. The frame with airtight chamber for the device.

Major benefit of the design of the device is the compatibility with different build plates. Initially the build plate base of the device is designed for standard medium sized building platform with dimensions of 250 x 250 x 36 mm and weight of 17 kg. This type of build plate is used in EOS M 290 PBF printer, which was used as a guideline in the design. However, it is possible to fit similar build plates with various thickness dimensions if the attachment screw holes are in the same place. Regarding different build plate area dimensions, the designed base is possible to be modified by adding screw holes to fit the new build plate dimensions.

The mechanism for rotating the build plate is assembled on an aluminum T-slot bar. The primary axle is suspended between two bearings, which are isolated from the rest of the frame with rubber mounts. Movement for the primary axis rotation is provided by a stepper motor and a reduction gear. The secondary axis is mounted perpendicular to the primary axis and rotated by a stepper motor and a belt drive with a gear ratio of 1:2.

Vibration for dislodging the powder was achieved with an eccentric steel weight mounted to the shaft of a DC motor. The frequency of the vibration can be adjusted by changing the output voltage of the power supply, while the amplitude can be changed by changing the dimensions of the eccentric weight. Vibration motor assembly is presented in Fig. 5.

Figure 5. Vibration motor assembly, with a DC motor, steel mounting bracket and an eccentric weight installed to its shaft.

As the goal of this project was to design a user-friendly device, the program code for the user interface was designed to be as simple as possible. The code consists of five functions: main function where the user is advised to choose a duration for the removal process between four different levels, and a function for each duration. This gives the user only the necessary controls: start, stop and duration.

Discussion

This work presented a design of a metal AM powder removal device. Advantages of this design are cost-efficiency and simple mechanism. In addition, this design is possible to be modified with relatively low effort as the aluminium profiles provide rails to adjust the location of the motors and axles to be suitable for various powder removal cases.

To further improve the device, a scale for measuring the amount of removed powder could be added. This would give more confidence to the user, since the device could inform the user that no more powder is being removed from the printed part after certain amount of time. The scale could also be used for optimizing support structures in terms of trapped build material powder, since the amount of removed powder could be quantified.

Another possible future improvement is to add a second way of introducing an impact to the build plate for dislodging build material powder. For example, a pneumatic cylinder with a striker can be added to the primary axis, providing a greater impact force alongside the vibration produced by the current solution.

The size of the chamber frame around the main mechanism could be made more compact as the depth does not necessarily need to be 700 mm as the workpiece does not need to be turned around 360°. It is enough if the part is rotated around 180°, because this would already enable moving the part to all needed orientations to make the removal efficient.

References

[1] J. Slotwinski and E. Garboczi, "Metrology Needs for Metal Additive Manufacturing Powders," *The Journal of The Minerals, Metals & Materials Society (TMS),* vol. 67, no. 33, pp. 538-543, 2015, [Online], DOI: 10.1007/s11837-014-1290-7.

[2] T. Hämeenaho, H. Tölander, E. Nordenberg, E. Komi, I. Rytkönen and J. Karjalainen, "ADDITIVE MANUFACTURING CENTER OF EXCELLENCE (AMCE) IN FINLAND," 2019, [Online], Available from: https://www.businessfinland.fi/4ada70/globalassets/finnish-customers/02-build-your-network/digitalization/hx-fighter-program/am-center-feasibility-study-2019-nov.pdf.

[3] A. Hussein, L. Hao, C. Yan, R. Everson and P. Young, "Advanced lattice support structures for metal additive manufacturing," *Journal of Materials Processing Technology,* vol. 213, no. 7, pp. 1019-1026, 2013, [Online], Available from: https://doi.org/10.1016/j.jmatprotec.2013.01.020.

[4] A. Townsend, N. Senin, L. Blunt, R. Leach and J. Taylor, "Surface texture metrology for metal additive manufacturing: a review," Precision Engineering, vol. 46, pp. 34-47, 2016, [Online], Available from
[5] Z. Chua, I. Ahn and S. Moon, "Process monitoring and inspection systems in metal additive manufacturing: Status and applications," International Journal of Precision Engineering and Manufacturing-Green Technology, vol. 4, no. 2, pp. 235-245, 2017, [Online], Available from: https://doi.org/10.1007/s40684-017-0029-7.
[6] B. Vayre, F. Vignata and Villeneuvea, "Identification on some Design Key Parameters for Additive Manufacturing: Application on Electron Beam Melting," Procedia CIIRP, vol. 7, pp. 264-269, 2013, [Online], Available from: https://doi.org/10.1016/j.procir.2013.05.045.

Self-Leveling Spreader Beam for Adjusting the Orientation of an Overhead Crane Load

Aleksi Kuuva[1,a], Sean Connor[1,b], Paavo Palomaki[1,c], Mikko Heliö[1,d], Panu Kiviluoma[1,e] and Petri Kuosmanen[1,f]

[1]Department of Mechanical Engineering, Aalto University, Finland

[a]aleksi.kuuva@aalto.fi, [b]sean.connor@aalto.fi, [c]paavo.palomaki@aalto.fi, [d]mikko.helio@aalto.fi, [e]panu.kiviluoma@aalto.fi, [f]petri.kuosmanen@aalto.fi

Keywords: Spreader Beam, Self-Adjusting, Remote Operation, Rotation of Load, Airborne Orientation Change, Under-the-Hook Device

Abstract

While the need to reorient crane loads while in-air exists, only a few products are available on the market which attempt to fulfill this specific purpose, but there exist inherent limitations. This study describes an under-the-hook device, that allows re-orientation of a load during an overhead crane lift. To develop such a device, product development methods were used to create, evaluate and narrow down different solution concepts for the problem. The resulting system structure was mechanically and electrically designed, and portions of the system were tested. A control logic for the operation of the product was developed, showing that proposed system has the potential to proceed to full size prototype phase. From product development perspective, this study presents a solution for mid-lift load rotation and guides the future development possibilities for the device.

Introduction

The overhead crane has been a tool used for industry even as far back through time as the Roman Empire [1]. The major purpose of these tools is to lift and move large, heavy objects. These machines vary in form depending on their application. Mobile cranes attached to road-legal vehicles, tower cranes used to build ever taller buildings in modern cities, and overhead cranes used inside industrial buildings are among those used most commonly today [2].

While hoisting and movement are carried out by the crane, additional tools have been developed for use with the machines to enhance their capabilities. One such additional tool is coined the "below-the-hook lifting device," or a BTH device for short. This is defined as a tool which is used to secure the payload and attach it to the crane's hoisting hook so that moving the object can be done safely for personnel and efficiently [3]. Common examples of BTH devices include coil hooks, gripping lifters, pallet lifters, and spreader beams and bars. The spreader beam is of key importance when lifting objects of greater length. This is a bar attached to the crane hook which provides multiple possible points for rigging to be attached, allowing for a more distributed load on the payload and an increase in stability of the system [4]. Existing versions of this design allow for adjustment of two to four hoisting points [5, 6].

Manipulation of a load once it is airborne can be of interest. This could simply mean changing its orientation. Examples of this exist in the form of die-turners and machines that complete the same process. With these machines, a strap is slung around the load when it is lifted. These straps are then fed through a pair of roller blocks such that they rotate the load over one axis of rotation [3], which resembles the motion of a workpiece in a lathe. Options which have the freedom to rotate a workpiece over two axes are not widely available.

Devices capable of rotating a load 360 degrees about one axis are available in the form of "die-turner" or "turnover" spreader beams [7]. This is achieved by feeding a continuous lifting strap through rollers and letting the load be cradled by the strap, allowing it to fall in a controlled manner

as it is rolled end over end. This approach does not allow for solid connections to the work piece. Methods like the spreader beam constructions [5, 6] allow for this solid connection to the workpiece.

In this study, system which has the capability of rotating a crane payload around two axes of freedom and can be adjusted remotely is developed, and its specifications described.

Methods

The primary goal of the development process is the creation of a BTH device capable of remotely controlling the rotating of a crane load about one or more axes. Operation is desired to be easy and safe. All motions of the frame in reaction to the changing orientation of the load should be made automatically. Control logic is therefore included as a key component of the solution.

Research was conducted into the state of the art and pre-existing solutions to the problem statement. The results of the research led to product-development-inspired ideation sessions, during which potential systems, components, and functionalities were proposed. The identified major subsystems and solutions are documented as a morphological table in Table 1. From this pool of ideas, the four most promising designs were further developed into detailed product proposals. The proposals were evaluated using the following criteria: 1. rotation along first axis, 2. rotation along second axis, 3. number of parts in assembly, 4. end user usability, 5. manufacturability, 6. ease of coding, 7. level of innovation.

Table 1. Morphological Table of Potential Components and Features for Novel BTH Device

Solutions →

Subsystems ↓

Support frame	 rectangular	 gimbal	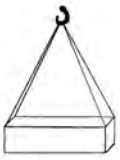 none	 arc-shaped	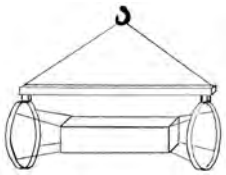 tubular
Sling shortening method	Screw	rope drum	twisting	pulley	gear
Number of lifting slings	3 pcs	4 pcs	8 pcs		
Degrees-of-freedom	1	2	3		
Hoist method	straps	chains	strings	cables	
Orientation sensing method	sensor on load	sensor in frame	inclinometers on the slings	camera on frame	
Powering method	battery on frame	cable to crane superstructure	cable straight from wall		

The concepts were further refined through iterative prototyping and validated with 3D modeling software. The concept to be developed has componentry based on the underlined subsystem solutions in Table 1.

Results

The product development methods outlined in the methods section culminate in the following description of a potential product design. Figure 1 describes the geometry of the product, with numbers indicating points of interest. This spreader beam design brings together the final decisions of the design phase. These include attempting to control an object with fixed lifting attachment points. Furthermore, the range of motion desired included two perpendicular axes of rotation.

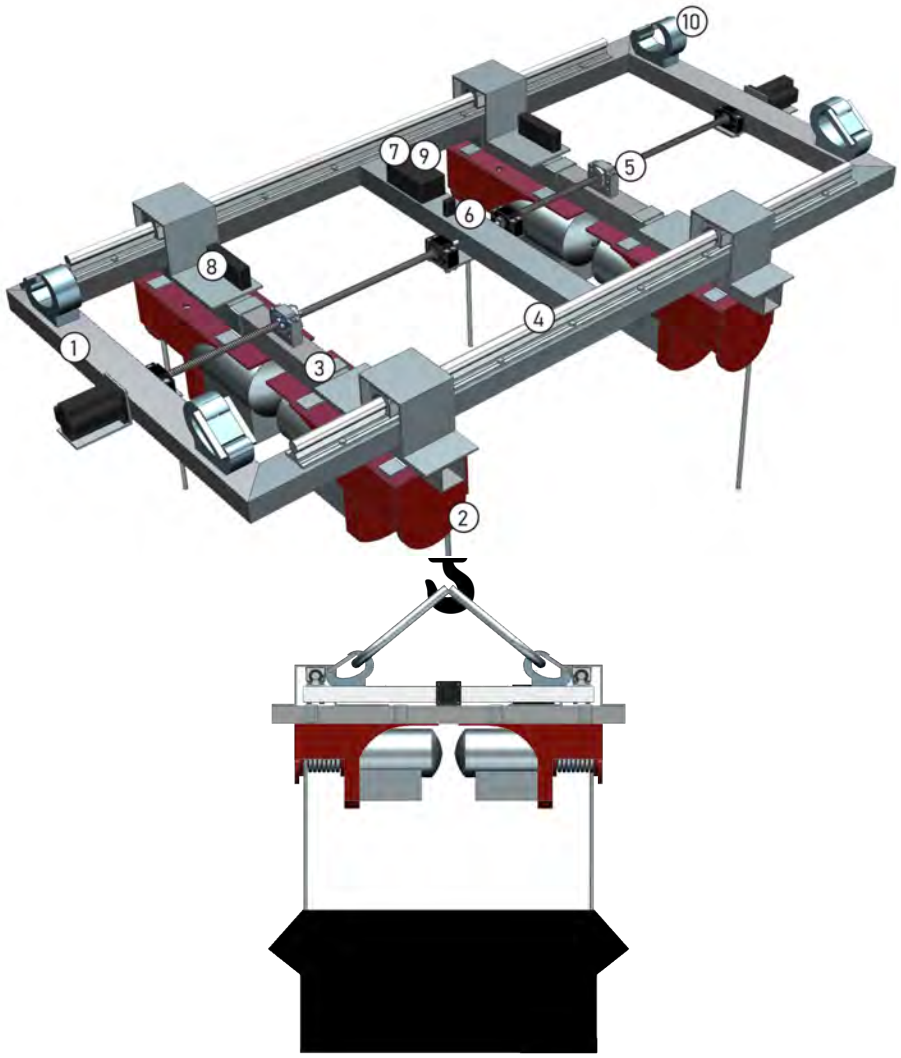

Figure 1. Image of the proposed adjustable spreader beam. Isometric view on the left, side view on the right. Points of interest (POI) include: 1. Steel frame, 2. Four electric winches, 3. Two linearly translating trolley assemblies, 4. Two rails, 5. Two stepper motor driven ball screw assemblies, 6. Frame mounted inertial measurement unit, 7. microcontroller, 8. Two relay modules, 9. Bluetooth receiver, 10. Four lifting eyes.

System Design. The primary frame is constructed out of steel tubing. Rotation of the load is achieved with four independently operable winches. Trolleys are attached to carts equipped with linear bearings which ride along rails mounted on the top side of the frame. Suspension of the frame utilizes lifting eyes attached to each corner. Stepper motors, along with ball screws, are used to translate the trolleys.

To ensure safety and reliable operation, the frame is to be kept level with the ground. While the winches are operated by user input the frame will be kept level with a controller automatically actuating the stepper motors and, therefore, the trolley positions relative to the crane hook.

Control. Operation of the winches is accomplished with the microcontroller mounted in the center of the frame. As shown in Figure 2 the microcontroller is controlled via Bluetooth from an external sender. The commands received by the main microcontroller are then interpreted and sent to the relay modules to operate the four winches based on what movement prompt the user has supplied.

The electric and control systems schematic displayed in Figure 2 details the connections and functionality of the two subsystems: the user-input device, and the spreader beam. All the systems presented in the diagram have been tested individually for functionality. To test the application of the user-input device, a smartphone was used with the rudimentary interface illustrated in the top left of Figure 2. Power is supplied to the system from an external 230 V source.

The four lifting winches installed under the trolleys are commercial winches, which are modified for the purpose by disassembling the control pendant. The control architecture of the pendants is rewired through two circuit boards hosting 8 digitally controlled relays each. These relays are controlled using a common microcontroller. This enables running the winches individually or at the same time. The winches are powered with standard 230 V / 50 Hz input, and the lifting hooks are moved at a constant speed of 4 m/min.

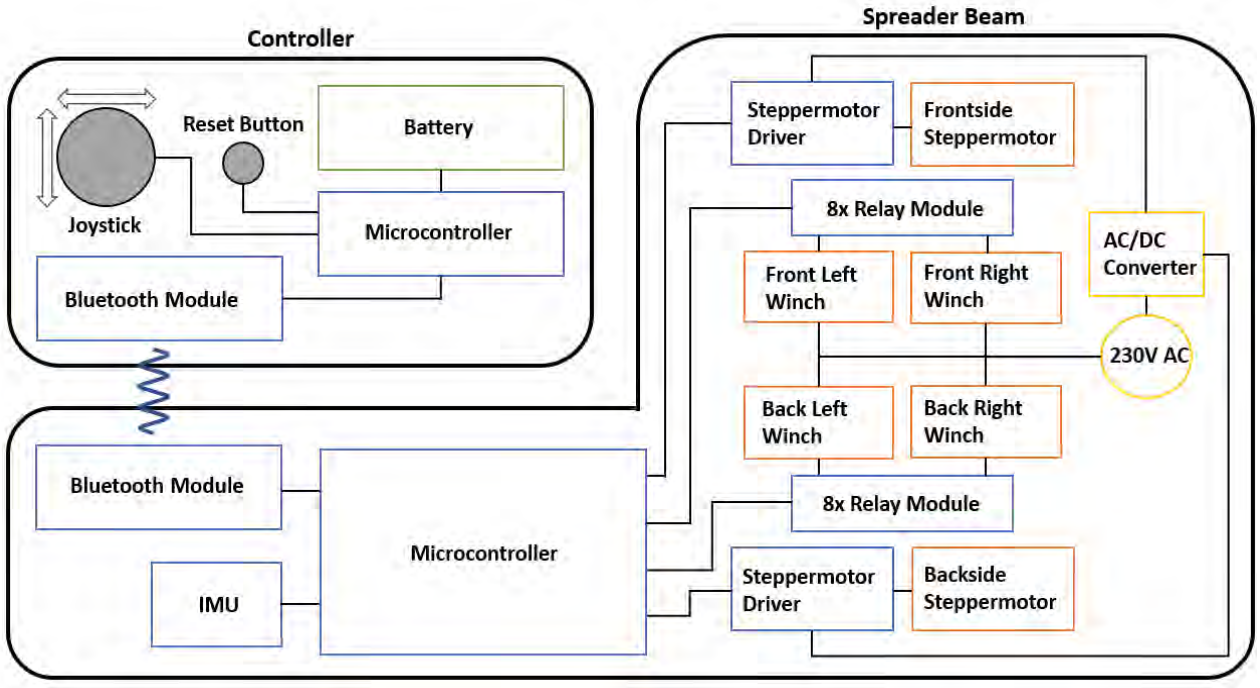

Figure 2. Schematic of the product's electrical system. The user interface device for the system is shown in the top left corner and the electric system mounted on the frame wraps around the image from lower left corner to top right corner. These two systems communicate through Bluetooth modules. Winches are controlled based on the user input from the controller. The steppers are controlled based on the IMU module output.

The winches are controlled wirelessly through use of a Bluetooth device compatible with the Bluetooth module of choice connected to the frame microcontroller. The handheld controller has a joystick functionality. Each movement of the joystick indicates a change in the orientation of the workload. This command is then interpreted, and the winches are lengthened or shortened accordingly. For tilting there are four different commands the controller can send, one for both rotation directions for each rotation axis. In addition to this, a reset button was added to the controller. The purpose of it is to level the load by first pulling all winches up to their minimum length and then lowering them by some set amount. This allows inbuilt limit switches in the winches to let the winches which have reached max up to disregard the "up" command until they are all in the same position, after which they are lowered to be attached to the load.

Automatic control of the trolley positions is achieved by implementing a control schema based on the data collected from the frame-mounted inertial measurement unit, IMU. This sensor produces a digital output based on the orientation of the frame. As the winches are adjusted to rotate the crane load, the center of gravity of the workpiece relative to the support connections may change. This change of balance can cause the frame to tilt in the direction of the center of gravity relative to its midline.

To bring the frame back into level, the trolleys are moved in an attempt to bring the center of gravity of the load in line with the crane hook. This is done by actuating the stepper motors, thus moving the ball screw assemblies and therefore the trolleys. Each stepper motor is controlled individually with PID controllers. The input for the controllers is the tilt angle of the frame, which is obtained from the MPU-6050 accelerometer/gyroscope sensor, and output is the movement of the trolleys.

The stepper motors include encoders, allowing the monitoring of their position by recoding the number of rotations that are made by the motor. This information combined with the tilt of the frame provided by the IMU allow the controllers to attempt to adjust the position of the trolleys to bring the frame into level. The most stable position for the trolleys is outboard of the lifting points on the load. Therefore, the zero position of the trolleys is at the full-out position. The controller attempts to move the center of gravity of the load back to the centerline of the frame by first moving the higher trolley toward the zero position if possible and lower towards centerline of the frame if not or the frame still is not level after moving the other trolley. This is to keep the trolleys as far apart from each other as possible, to keep the aforementioned stability of the load.

The controller is tuned so that the trolleys are moved slowly, in order to minimize the effect of the movements of the frame on the output of the IMU. In this way, the system is assumed to operate in a quasi-static state. Also, after reaching a horizontal orientation, the stepper motors are not actuated again until there exists an angle greater than a small threshold value to minimize effect of noise. This is done to avoid running the steppers back and forth with low frequency. In addition to this, the automatic adjustment of the angle of the frame is not done when the crane is in motion.

A saturation of 8 kHz is set for the input signal of the steppers so that the maximum speed is 600 rpm, producing a torque of 1.2 Nm. The ball screws have a pitch of 4 mm This, combined with the stepper motor's maximum speed yields a trolley movement speed of 2.4 m/min. Selected motors are running with 36 V power supply and closed-loop stepper drives.

Analysis. During the individual subsystem experiments, an Arduino Mega was used as microcontroller. It was observed that an Arduino is not a suitable controller for the system, as the selected stepper motor requires a high-frequency series of commands to rotate. The stepper was run separately without a problem, but after adding the calculation of the tilt angle from the IMU raw values, the stepper movement became unstable. This was due that it took the controller 15 ms to read the angle, which caused too much delay in the loop. A controller which can execute parallel processes simultaneously is needed for this application.

The working principle of the Bluetooth controller was tested by building a mobile phone app to connect to the microcontroller and simulate the output of moving a joystick. The winch motor control experiment proved successful, however, considering the use case, the mobile phone controller likely should be replaced with a more durable, universal, and user-friendly physical joystick controller.

The commercially available winches used in experimentation proved to be more than adequate at only a modest price. They included their own control pendants, high lifting capacity, and max up and max down limit switches. Developing a stripped-down version for the product could reduce cost and minimize extra cables and wiring which, while needed for a pendant installation are unneeded for this control schema, thus simplifying the electronics of the system.

Use of a self-leveling spreader beam, such as presented in this paper, could enable more diverse use of an overhead crane. Different pick-and-place and assembly operations could be achieved, when the payload can be rotated along 3 axes. There is no product on the open market available which can offer the same functionality. Thus, this product poses a significant, novel change to the current functionality of crane operation.

Based on the original problem statement, the resulting design can be considered a success based on the following criteria. While maximum angle of rotation of the load is limited, the product offers more than one axis of rotation of the load, thus allowing complex manipulation of the load in a manner not otherwise available as a BTH device. The complexity of the system is relatively low. There is the possibility to expand the design to an H-frame as described in the introduction, thus increasing the devices ability to handle complex manipulations of the load. Finally, the controls are simple enough that when the BTH device is added to a crane setup, no interaction between the frame operation and the crane operation is needed, thus making the installation possibilities of the device myriad.

Discussion

The next steps for the development of the self-leveling spreader beam would be to build a working prototype and test it. The performance of the device should be evaluated quantitatively based on its ability to perform in a timely manner, and how large the manipulations of the load are measured to be. Additionally, quantitative analysis of the device can be recorded by implementing user tests with industry experts who regularly use cranes and BTH machinery.

Suggestions for potential future steps can be made based on test results include:

1. Add linear movement perpendicular to the existing direction of the trolley moment for each winch, thus allowing stabilization of the frame along two axes of rotation
2. Develop a closed loop control system where the angle of the payload is known with inclinometers installed to the winch wires
3. Optimize the frame structure for maximum strength-weight ratio
4. Add control logic which stops adjustment of the trolleys when the main crane is moved
5. Power the product with onboard installed batteries
6. Determine the appropriate microcontroller capable of providing the high-frequency commands to the stepper motors, as well as accepting the user input and actuating the winches without running into parallel process problems.
7. Develop filter for IMU signal to reduce effect of noise on the performance of the system.

References

[1] Crane (machine). (2013, July 4). *New World Encyclopedia,* . Retrieved 08:33, March 4, 2020 from //www.newworldencyclopedia.org/p/index.php?title=Crane_(machine)&oldid=970918.

[2] "Top 7 Types of Construction Cranes: TNT Crane & Rigging." *TNT Crane*, 20 Mar. 2017, www.tntcrane.ca/top-7-types-of-construction-cranes/.

[3] Close, Mike CloseMike. "What Is a Below-the-Hook Lifting Device? Definition, Types, and Design." *Mazzella Companies*, 30 Aug. 2017, www.mazzellacompanies.com/Resources/Blog/below-the-hook-lifting-device-definition-types-design.

[4] Sparta. "Why Do I Need a Spreader Bar?" *Sparta Engineering*, 13 Feb. 2016, www.spartaengineering.com/need-spreader-bar/.

[5] "Aardwolf Spreader Bar - 3.5 Tons." *Diamond Tool Store*, www.diamondtoolstore.com/aardwolf-spreader-bar-3-5-tons/.

[6] "H Frame Lifting Beam." *Indiamart.com*, www.indiamart.com/proddetail/h-frame-lifting-beam-16343947097.html.

[7] "Turnover Spreader Beam." *PFEIFER Worldwide*, www.pfeifer.info/en/products-services/products/lifting-and-turning-devices/spreader-beams/turnover-spreader-beam.html?force_sid=s9np4ifbal9h4gl7v5u7paj0eq.